NTNU
Norwegian University of
Science and Technology

Impacts of Mechanical Properties and Blade Morphology on Seaweed Hydrodynamics in Steady Flow

Karoline Sjødal Olsen

Marine Technology
Submission date: June 2017
Supervisor: Dag Myrhaug, IMT

Norwegian University of Science and Technology
Department of Marine Technology

NTNU Trondheim
Norwegian University of Science and Technology
Department of Marine Technology – Group of Marine Structures

MASTER THESIS IN MARINE TECHNOLOGY

SPRING 2017

FOR

STUD. TECHN. KAROLINE SJØDAL OLSEN

IMPACTS OF MECHANICAL PROPERTIES AND BLADE MORPHOLOGY ON SEAWEED HYDRODYNAMICS IN STEADY FLOW

The interaction between aquatic biological systems and their physical environment represents a complexity which is important to understand for sustainable management of aquatic environments. In order to learn more about the complexity of the processes that take place in such environments, the knowledge from different disciplines have to be taken into account, from e.g. engineering, biology and ecology. Several issues need to be considered, such as the biomechanical properties of the plant, the complex fluid flow involving turbulent processes, and scaling issues related to laboratory experiments.

The thesis will focus on various issues of the representation of vegetation-flow interactions in laboratory experiments.

The student shall:

1. Give a literature review of flow and aquatic vegetation interaction.
2. Give the theoretical background for the vegetation-flow interaction, the hydrodynamic forces and scaling issues.
3. Perform, present and discuss results from preliminary flow experiments in the flume in order to map the flow conditions to be used in the final vegetation-flow interaction tests.
4. Perform, present and discuss results from final vegetation-flow interaction experiments.

The work scope may prove to be larger than initially anticipated. Subject to approval from the supervisor, topics may be deleted from the list above or reduced in extent.

In the thesis the candidate shall present her personal contribution to the resolution of problem within the scope of the thesis work.

Theories and conclusions should be based on mathematical derivations and/or logic reasoning identifying the various steps in the deduction.

The candidate should utilize the existing possibilities for obtaining relevant literature.

The thesis should be organized in a rational manner to give a clear exposition of results, assessments, and conclusions. The text should be brief and to the point, with a clear language. Telegraphic language should be avoided.

The thesis shall contain the following elements: A text defining the scope, preface, list of contents, summary, main body of thesis, conclusions with recommendations for further work, list of symbols

and acronyms, reference and (optional) appendices. All figures, tables and equations shall be numerated.

The supervisor may require that the candidate, in an early stage of the work, present a written plan for the completion of the work. The plan should include a budget for the use of computer and laboratory resources that will be charged to the department. Overruns shall be reported to the supervisor.

The original contribution of the candidate and material taken from other sources shall be clearly defined. Work from other sources shall be properly referenced using an acknowledged referencing system.

Deadline: 11.06.2017

Supervisors: Post.doc. Pierre-Yves Henry, Department of Civil and Environmental Engineering
Professor Dag Myrhaug

Dag Myrhaug
Supervisor

Preface

This master thesis is written as the final work of an integrated master in Marine Technology at the Norwegian University of Science and Technology, NTNU, in Trondheim Spring of 2017.

I chose to write my master thesis within hydrodynamics of aquatic vegetation, because it is a new field of research. Research on aquatic plants may bring new knowledge on how to preserve future resources in a better way, and I find it motivating.

The journey of working with the master thesis has been challenging, but also very rewarding. I have had many obstacles to overcome understanding the proper way to perform laboratory work in order to obtain valuable results, implement theory and understand the mechanisms of a new field of research. It has been a great journey!

Trondheim, 10.06.2017

Karoline Sjødal Olsen

Acknowledgment

I would like to thank my co-supervisor Pierre-Yves Henry for his help, advise and guidance throughout this master thesis. I would have not been able to understand the complexity of laboratory work in connection with implemented theory on the hydrodynamics of aquatic flow without you. I would also like to thank my supervisor Dag Myrhaug for kind words of encouragement when times got stressful, and for inputs and help in understanding the hydrodynamic processes interfering with flexible organic structures. Lastly, I would like to thank my boyfriend, Christian Kosacki, for tremendous support and making everyday a little bit more fun.

K.S.O.

List of symbols

A	$[m^2]$	Plant area
A_p	$[m^2]$	Frontal projected area
b	[m]	Beam width
B	[N]	Buoyancy force
c	[m/s]	Speed of sound
C_a	[-]	Cauchy number
C_D	[-]	Drag coefficient
$C_{D,friction}$	[-]	Friction drag coefficient
$C_{D,pressure}$	[-]	Pressure drag coefficient
C_L	[-]	Lift coefficient
d	[m]	Small plant scale
D	[m]	Characteristic length of an object subject to drag force
E	$[Nm^{-2}]$	Young's modulus.
EI	$[Nm^2]$	Flexural rigidity
F_b	[N]	Bending (reaction) force
f_b	[N]	Vertical Buoyancy force
F_B	[N]	Buoyancy force
f_D	[N]	Drag force
F_D	[N]	Drag force
$F_{D,friction}$	[N]	Friction drag
$F_{D,pressure}$	[N]	Pressure drag
F_G	[N]	Gravity force
F_L	[N]	Lift force

f_t	$[s^-1]$	Frequency transmitted
F_T	[N]	Tensile (reaction) force
F_{x0}	[N]	Drag force
Δf	$[s^-1]$	Frequency shift
g	$[m/s^2]$	Gravitational acceleration
H	[m]	Height of vegetation
I_2	$[m^4]$	The second moment of inertia
l	[m]	Blade length
l_e	[m]	Effective blade length
L	[m]	Large plant scale length
R	[m]	Radius of a curvature at a point where bending is defined
R_n	[-]	Reynolds number
s	[m]	Blade length
s^*	[m]	Blade length at arbitrary position
U	[m/s]	Flow velocity
t	[m]	Thickness of the beam
V	[N]	Blade-normal restoring force due to stiffness
V_p	$[m^3]$	Volume of plant
ϵ	[-]	Strain (relative elongation)
ρ	$[kg/m^3]$	Density of the fluid considered
ρ_p	$[kg/m^3]$	Density of the plant
ρ_v	$[kg/m^3]$	Density of beam
λ	[m]	The distance from the bed surface to the point where the fluid resultant force acts
ν	$[m^2 s^-1]$	Kinematic viscosity of water

θ	[rad]	Local bending angle relative to the vertical position
μ_{B-G}	[-]	Similarity number from buoyancy and gravitational forces
μ_{D-B}	[-]	Similarity number from drag and buoyancy forces
μ_{D-b}	[-]	Similarity number from drag and bending (reaction) force
S_t	[-]	Strouhals number
f_n	[Hz]	Natural frequency
f_v	[Hz]	Shedding frequency
ω_n	[rad/s]	Natural frequency in rad/s
ω_v	[rad/s]	Shedding frequency in rad/s
U_∞	[m/s]	Incident flow velocity
U_e	[m/s]	Tangential velocity
k	[N/m]	Stiffness factor
m	[m]	Mass
m_a	[m]	Added mass
τ_{turb}	$[(m/s)^2]$	Reynolds stress tensor
u'	[m/s]	Fluctuating velocity in x-direction
$\bar{u}$	[m/s]	Mean velocity in x-direction
v'	[m/s]	Fluctuating velocity in y-direction
τ_w	$[(m/s)^2]$	Wall shear stress
f	[m]	The operating frequency of the ADV

Acronyms

ADV Acoustic Doppler Velocimetry

SNR Signal-to-Noise-Ratio

PIV Particle Image Velocimetry

COR Correlation level of the ADV

Abstract

Global environmental changes are a well known phenomenon affecting the climate around us. The challenges the world face in the coming 30 years regarding food production, climate change and adaption to new environments will have a tremendous impact on the way we live. The interactions between aquatic biological systems and their physical environment can help increase the information on different aspects of these changes. The complexity of the aquatic systems help with absorption of carbon dioxide, wave damping at exposed shores and as a future food source. All of these advantages can help to diminish these changes in a sustainable way. Expanding the knowledge around these subjects will increase the probability of solving the coming challenges.

In this thesis the aspect of plant-flow interactions is investigated. Surrogate plant models with different materials and simplified plant shape were used to mimic real plant behaviour exposed to fluid flow. Drag forces on the plant surrogate are also tested experimentally. A laboratory flume tank was used for the model tests. In order to understand the flow behaviour several preliminary experimental tests were performed to map the flow conditions. Flume floor measurements, velocity tests, water elevation tests and head loss were investigated. Acoustic Doppler Velocimetry was used to observe the velocity profiles occurring in the flow both in vertical direction and across the cross-sections of the flume. The velocities were recorded at velocity *0.34 m/s*. Measurements were recorded from point *423 cm* to *1400 cm*. The vertical velocity profiles from point *1023 cm* indicated inaccuracies at the top half of the water column. These inaccuracies can occur from eddies in the flow creating second-order effects disturbing the profile. The cross-sectional profiles indicated an inaccuracy at point *1023 cm*, but showed an improvement further down the flow at point *1400 cm*. This inaccuracy can be caused by second-order current by changes of the flume floor throughout the flume. The velocity profile were also compared to previous velocity profiles obtained from the preliminary testing in Fall 2016. The turbulent Reynolds stresses were mapped at these points, and the findings undermined the assumption of second-order effects. The surrogate models were made using a plexiglass mould of a simplified shape of the kelp *Laminaria Digitata*. Three models were made in three different silicone materials ranging in shore hardness from 20A-90A.

The plant models were tested with five different velocities from *0.05 m/s* to *0.34 m/s* to observe plant-flow interactions and drag forces. The plant model surrogate 60A was the only one investigated regarding drag forces, because it was the surrogate model without air bobbles and holes in the silicone structure. The plant-flow interaction were recorded with cameras at different points outside the flume. The results of the plant-flow interaction tests indicated different behaviour for the surrogate models. Surrogate 20A, the most flexible model, streamlined for the lowest velocity of *0.05 m/s* and the stiffest model surrogate 90A only streamlined at the highest velocity of *0.34 m/s*. Surrogate 20A was also the only model significantly moving crosswise in the flume, which can possibly be linked to the second-order currents. From the videos recorded of the model oscillating frequencies of the plant stems were observed. The frequencies observed seemed to converge towards a similar value around *1.5 Hz*. This is unfamiliar behaviour, and may be an indication of the lock-in effect of vortex-induced vibration. The vortex shedding frequencies were plotted against the frequencies of the plant models, but the plot did not indicate a lock-in effect. Therefore, a suggestion that the blade of the plant may be the dominating factor was proposed. The undulating of the blade creates forces that cause the stem to oscillate, and it is therefore maybe not affected by vortex-induced vibration. This argument will need further analysis to be confirmed. The drag forces were inside a reasonable range expected by such a plant model shape, but did not follow the rule of increasing linearly with velocity squared. This is maybe caused by the Reynolds number not being significantly high. In conclusion, plant-flow interactions are complex processes that needs further investigations to confirm the finding from such experimental research as this. The model tests indicated that all the models streamlined as a way to minimise drag forces in the flow. This is confirmed by previous studies. The oscillations of the stem may be dependent on the blade motions. The behaviour of the plant models are affected by changes caused by second-order effects in the flow, especially the most flexible plant model. Further research is needed on plant-flow interactions to confirm the finding in this thesis.

Sammendrag

Globale miljøendringer er et velkjent fenomen som påvirker klimaet rundt oss. Utfordringene verden står overfor i de kommende 30 årene innen matproduksjon, klimaendringer og tilpasning til nye miljøer, vil få stor innvirkning på måten vi lever. Samspillet mellom akvatiske biologiske systemer og deres fysiske miljø kan bidra til økt informasjon rundt ulike aspekter ved disse endringene. Kompleksiteten i akvatiske systemer bidrar til absorpsjon av karbondioksid, bølgedemping ved utsatte kyster og som fremtidig matkilde. Alle disse fordelene kan bidra til å redusere disse endringene på en bærekraftig måte. Å utvide kunnskapen rundt disse fagområdene øker sannsynligheten for å løse de kommende utfordringene.

I denne oppgaven undersøkes plante-vannstrøm-interaksjoner. Surrogatplantemodeller med forskjellige materialer og forenklet planteform ble brukt til å etterligne reell planteadferd eksponert for væskestrøm. Drag krefter eksponert fra vannstrømmen på planten ble også testet eksperimentelt. En laboratoriestrømmningstank ble brukt til modelltestene. For å forstå strømningsadferden ble flere eksperimentelle tester utført i forkant for å kartlegge strømningsbetingelsene. Bunnmålinger av tanken, hastighetsmålinger, vanndybdetester og energitap ble undersøkt. Et måleinstrument kalt akustisk doppler velosimeter ble brukt til å observere hastighetsprofiler som forekommer i strømmen, både i vertikal retning og over tverrsnittene av vannstrømmen. Hastighetene ble registrert ved hastighet $0{,}34\ m\ /\ s$. Målinger ble registrert fra punkt $423\ cm$ til $1400\ cm$. I de vertikale hastighetsprofiler i punkt $1023\ cm$ ble det observert unøyaktigheter i toppen av vannsøylen. Disse unøyaktighetene kan oppstå fra virlinger i strømmen som skaper andreordenseffekter som forstyrrer hastighetsprofilen. Tverrsnittsprofilene indikerte en unøyaktighet ved punkt $1023\ cm$, men viste en forbedring videre nedover strømmen ved punkt $1400\ cm$. Denne unøyaktigheten kan også være forårsaket av andreordenseffekter eller endringer nedover tankbunnen. Hastighetsprofilen ble også sammenlignet med tidligere hastighetsprofiler fra eksprimentelltesting i prosjektoppgaven høsten 2016. De turbulente Reynolds skjærspenningene ble kartlagt på disse punktene, og funnene underbygget antagelsen om andreordenseffekter. Surrogatmodellene ble laget ved hjelp av en plexiglassform av en forenklet form av taren *Laminaria Digitata*. Tre modeller ble laget i tre forskjellige silikonmaterialer med forskjellig hardhet fra 20A-90A.

Plantemodellene ble testet ved fem forskjellige hastigheter fra $0{,}05\ m\ /\ s$ til $0{,}34\ m\ /\ s$ for å

observere plante-vannstrøm-interaksjoner og dragkrefter. Plantemodellen surrogat 60A var den eneste som ble undersøkt ved dragmålinger, fordi den var det eneste surrogatet uten luftbobler heller hull i silikonmodellen. Plant-vannstrøm-interaksjonen ble registrert med kameraer på forskjellige punkter utenfor strømingstanken. Resultatene fra samspillet mellom plante-vannstrøm-interaksjonen indikerte forskjellig oppførsel for de ulike surrogatmodellene. Surrogat 20A, den mest fleksible modellen, strømlinjet seg i strømmen allerede for den laveste hastighet på $0{,}05\ m/s$ og den stiveste modellen surrogat 90A strømlinjet seg bare ved høyeste hastighet $0{,}34\ m/s$. Surrogat 20A var også den eneste modellen som beveger seg vesentlig i tverrsnitt i strømmen, som muligens kan knyttes til andreordeneffekter. Fra videoene av modellen, ble frekvensene til plantestilkene observert. Frekvensene konvergerte mot en lignende verdi rundt $1.5\ Hz$. Dette er et ukjent bevegelsesmønster, og kan være en indikasjon på lock-in-effekten av virvel-induserte vibrasjoner. Virvelavløsningsfrekvensene ble plottet mot frekvensene til plantestilkene, men plottet viste ingen lock-in-effekt. Derfor ble det foreslått at plantens blad kan være den dominerende faktoren for frekvensen til plantestilken. Bølgen av bladet skaper krefter som forårsaker at stilken oscillerer, og er derfor kanskje ikke påvirket av virvel-induserte vibrasjoner. Dette argumentet vil trenge ytterligere analyse for å bli bekreftet. Dragkreftene var innenfor et fornuftig område som forventes av en slik plantemodell, men fulgte ikke regelen med å øke lineært med kvadratet av hastigheten. Som konklusjon er plante-vannstrøm-interaksjoner komplekse prosesser som trenger ytterligere undersøkelser for å bekrefte funnene fra slik eksperimentell forskning som dette. Modeltestene indikerte at alle modellene strømlinjeformet seg som en måte å minimere dragkreftene i vannstrømmen. Dette bekreftes av tidligere studier. Oscillasjonene til stilken kan være avhengig av bladbevegelsene. Oppførselen til plantemodellene påvirkes av endringer som skyldes andreordens effekter i strømmen, særlig den mest fleksible surrogatmodellen. Videre forskning er nødvendig på plante-vannstrøm-interaksjoner for å bekrefte funnene i denne oppgaven.

Contents

Chapter 1

Introduction

Global environmental changes are a widely recognised phenomena. The effects will likely modify the marine life on dramatically over the next decades (Seckbach et al., 2010). Aquatic biological systems offer food and shelter for marine life such as fish, and are actively lowering global warming and climate change by absorbing carbon dioxide from the atmosphere. Aquatic vegetation may contribute as a valuable food source in the future also, as it is rich in protein and exists in abundance in the ocean.

When the environment changes knowledge of aspects that influence these changes, such as aquatic plants, will become important. Having said this there exists a lack of knowledge on the effects of flowing water on submerged aquatic plants, physical forces and wave action (Miler et al., 2014). Physical hydrodynamic forces in the fluid flow highly determine the plant distribution, nutrition, light availability and oxygen levels in the water. Investigating how these forces interact with the aquatic vegetation can give further knowledge on how the plant is likely to behave if a change in its environment should occur. However, investigating plan-flow interactions is a complex process, and several difficulties needs to be faced in order to investigate such systems.

Figure 1.1: Forest of the kelp Laminaria Digitata.

1.1 Background

We live in a world with a constant need of food supply, finding new methods of taking advantage of resources we have and at the same time struggle with the issues of climate change. Aquatic vegetation, like the kelp *Laminaria Digitata*, may be one of the solutions to these problems, as seen in Figure 1.2. The research carried out in this master thesis is based on a simplified model of this kelp, and brings knowledge on experimental research of the plant-flow behaviour. The focus until now have been in the field of biology, but are slowly moving towards more engineering based fields like hydrodynamics of aquatic vegetation. The need for more information on these hydrodynamic interactions are increasing.

Aquatic vegetation makes up an essential part of the coastal ecosystems and is found in abundance along most shores in the world. This is why utilising these plants becomes important when investigating new types of resources. In the following sections the benefits of aquatic plants are presented. The information provided are taken from the book by Seckbach et al. (2010) unless other references are stated. This will give a foundation for why investigating aquatic plants are important regarding sustainable resources of the future. The following sections are mostly based on the research carried out during the project thesis in Fall 2016.

Figure 1.2: The kelp *Laminaria Digitata* from Iceland dried as a food snack (Romsdals-Budstikke, 2015).

Food source

Aquatic plants are primary producers. They use photosynthesis to produce energy to grow and give oxygen to the environment around them. They are highly productive, which make them excellent for farming as a food source, and to not require much care in terms of fertilisers. They also store large amounts of nitrogen and carbon that can helping the environment surrounding them (Tiwari and Troy, 2015). Approximately 842 million people suffer from hunger worldwide, according to the United Nations and The Food and Agricultural Organisation (Tiwari and Troy, 2015). The production of food needs to increase by approximately *60%* by 2050 to meet the growing demand. The ocean holds valuable resources, but are barely taken advantage of today. The research of Tiwari and Troy (2015) presents that most seaweeds are edible and contain important nutrients like vitamins, minerals, essential fatty acids and proteins. Around 13 million tons of wet seaweed are harvested each year, mostly in Asia. In their natural habitat seaweed grow in abundance, meaning that the amount is almost unlimited. Even when farmed, it does not need any fertilisers or cleaning of water. This makes the environmental impact minimal. Even though the food source seems promising, we are not utilising the resource. Developing new technology making harvesting, cultivation and processing accessible are the first issues that needs to be investigated. This information builds a foundation for why utilising aquatic vegetation as a sustainable resource seems promising.

Energy source

The research of Seckbach et al. (2010) presents that most biofuels (biodiesel) produced in Europe origins from land based plant oils. As a consequence food prices have risen on basic staple foods, and the blame is given to the countries choosing to produce biofuels rather than food. This has given biofuels a bad reputation, as it takes away from the already strained food crops in the world. A solution to this problem may be to produce biofuel from marine algae. The yield to produce biofuels from algae is high. A comparison with other plants oil yields are shown in Table 1.1. More knowledge on utilisation of aquatic plants as biofuels are needed to confirm this resource as a sustainable energy source.

Table 1.1: Overview of various yields of plant oils in litre per hectare (Seckbach et al., 2010).

Crop	Oil (l/ha)
Castor	1,413
Sunflower	952
Safflower	779
Palm	5,950
Soy	446
Coconut	2,689
Algae	100,000

Climate change

As mentioned, aquatic vegetation has great potential for breaking down CO_2, but is also vulnerable to climate change. This plays a crucial role in how we can find ways to use and harvest aquatic plants without destroying the environment it lives in. When the ocean temperatures rise the species will relocate to find more suitable habitats. Several studies have investigated if climate change may have an impact on aquatic vegetation. Figure 1.3 shows growth testing of one type of aquatic plant with different CO_2 concentrations. The investigations carried out by Seckbach et al. (2010) concludes that physiological responses of seaweed to the higher concentrations of CO_2 in the oceans are highly variable. The tests performed showed growth were both inhibited, enhanced, or not affected at all by the increase in CO_2. In other words, this means that there is a need for more research on the impact increasing atmospheric CO_2 concentrations have on marine vegetation. Aquatic vegetation can also help dampen waves and flooding at exposed shores which may diminish future environmental changes at exposed coastline (Henry, 2016).

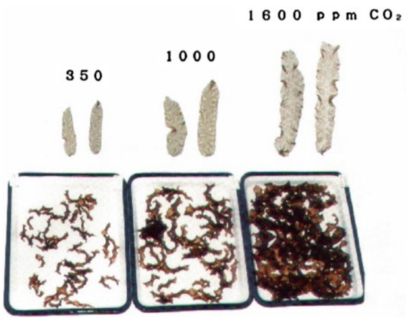

Figure 1.3: Growth testing on the aquatic plant *Porphyra yezoensis* at different CO_2 concentrations. *50* juvenile plants about *5 mm* long at the beginning were tested. Each of them germinated in the same way. The photo is taken after *20* days of growth (Seckbach et al., 2010).

The kelp *Laminaria Digitata*

This section presents brief information on the kelp $LaminariaDigitata$ its benefits, and gives support on why this type of aquatic plant is of interest in this field of research.

The distribution of the large brown algae *Laminaria Digitata* stretches from the Arctic, to the east coast of North America and even to the west coast of France (Sjøtun et al., 2004). There are limitations to the distribution in specific areas with too high temperatures in both parts of the North-Atlantic, but overall the distribution is extensive. For this reason utilising this kelp as a resource is wise. In mature plants the rate of growth is adjusted by the seasons and has been tested at locations in both Norway and France (Sjøtun et al., 2004).

In relatively wave-swept areas along the coast of Norway, *Laminaria Digitata*, are known to have the highest occurrences. With that being said, it is beneficial to investigate the behaviour as it can contribute to better utilisation of these types of resources in Norway. An illustration of the kelp *Laminaria Digitata* is found in Figure 1.4. The plant has a large blade that is attached to a single stipe with a holdfast at the bottom (Paul and Henry, 2014). The blade can grow up to 2 m in length and does not have a midrib. The surface is smooth and glossy, and the colour of the plant is brown. The tip of the blade is prone to being ripped due to exposure to wave motions inshore. The blade is slightly tapered towards the tip and this is likely why it is prone to ripping. In this thesis the kelp i substituted by a simplified surrogate model, and will be further explained in Section 3.4.

Figure 1.4: The large brown algae *Laminaria Digitata* (Bollner, 2006).

1.2 Literature review

In the Fall of 2016 a literature review was carried out in the project thesis prior to this master thesis. The following section is a brief summary on the review given in the project thesis, with some supplements in the area of experimental research on aquatic vegetation. The information presented covers similar research performed prior to this thesis, but one must highlight that this field of research is new, so direct comparisons to previous works are not possible. This literature review is a product of continuous research throughout this and the past semester, and contains the most significant findings related to the hydrodynamics of aquatic vegetation. The relevant theoretical findings will be presented in Chapter 2.

This master thesis is an extension of the research carried out by Henry (2016). His research presents the importance of plant biomechanics in the hydrodynamics of vegetated flow, and represents the basis for experimental research carried out in this thesis. His studies on experiments containing surrogates of the kelp *Laminaria Digitata* show that the hydrody-

namic forces experienced by aquatic plants depend on their biomechanical properties, such a buoyancy and stiffness. He also concludes that further research is needed to confirm if the observations represents the natural behaviour of the plant under the given hydrodynamic forces. Research performed in this master thesis will continue the work of Henry (2016), and help provide more information to the field of hydrodynamics of aquatic vegetation.

Ennos (1999) investigates the need for biomechanical research on plants to cover the field of fluid dynamics as comprehensively as solid mechanics. The topic of hydrodynamic drag on plants is widely discussed in his paper as it can give valuable information on the mechanisms the plant uses to minimise drag. He concludes that more knowledge on the hydrodynamics of aquatic plants will help us answer important evolutionary questions both from the past and the future.

Miler et al. (2012) carried out experimental studies on biomechanical properties of aquatic plants in correlation with plant-flow interactions. This is one of the few studies similar to the study performed in this thesis. The plant stems of four different river macrophyte species were investigated in a laboratory performing tests on tension, bending and cyclic loading. The findings supported previous theories saying that the biomechanical properties of a plant complements the forces acting in the area it operates in. Miler et al. (2012) suggests making a database of biomechanical characteristics of freshwater macrophytes.

Another similar study is (Albayrak et al., 2014). The paper is the first to report a systematic study of statistical characteristics of plant-flow interactions at leaf, stem and shoot scales. They analysed values such as mean values, standard deviation and transfer functions among others. The values were analysed in the light of drag, turbulence and biomechanics. This study also concludes that biomechanical properties are extremely important when investigating plant behaviour, and defines the motion in some way.

The last research article covering similar experiments is (Miler et al., 2014) studying biomechanical properties and morphological characteristics of lake and river plants. Stems of eight species were analysed to investigate the differences between river and lake specimens, the influence of the changing seasons and change of biomechanical and morphological properties between the species. The study concludes that seasonal changes affect river macrophytes, and that there exists differences between river and lake species. Making a database of freshwater plant properties are also suggested.

Schiel and Foster (2015) provides an overview of different aspects of giant kelp forests ranging from biology, ecosystems, human usage to flow-interactions with current and wave motions. Figure 1.5 gives a schematic overview of kelp mechanics in correlation with fluid flow. From the figure it is observed that water motions have likely influenced many aspects of aquatic plants including morphology, physiology, demography and probably the evolution too. To understand the complexity of the life of kelp and other aquatic vegetation, one needs to investigate the nearshore environments they live in. The investigations needs to pay particular attention to the physical disturbances that affects the plants in their own habitat.

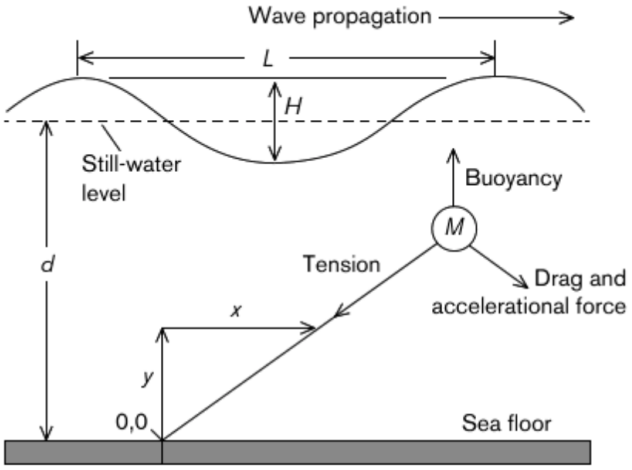

Figure 1.5: Numerical model of the kelp mechanics represented schematically (Schiel and Foster, 2015).

As stated by Koehl (1999) *«In some ecological context, "bad" mechanical designs can fare quite well.»*. In his research he found that there is no requirement for an organism to have "good" mechanical design in order to survive. New research found on the influence of water motion on growth rate *Laminaria Digitata* by Kregting et al. (2013) suggests that the growth rate may depend on the water motions, with plants being smaller and tougher in wave-swept areas. These findings are in contrast to previous studies showing no direct influence on growth from water motion. The study also found that the *Laminaria Digitata* had reduced growth rate both in the highest current flow and when exposed to waves.

Hurd (2000) also investigates how the hydrodynamic environment influence aquatic vegetation. Aquatic plants depend on seawater turbidity in order to get enough light and carbon uptake. Figure 1.6 shows the velocity boundary layer and velocity profiles in a flow over a flat plate. The velocity fluctuations that arise in the three dimensional flow may be ob-

served as discrete moving parcels of water, also called eddies, and move between fluid layers. When these eddies are carried towards the plant they can contain nutrient-rich seawater. The mechanism are vital for aquatic vegetation, and are further explained in Chapter 2.

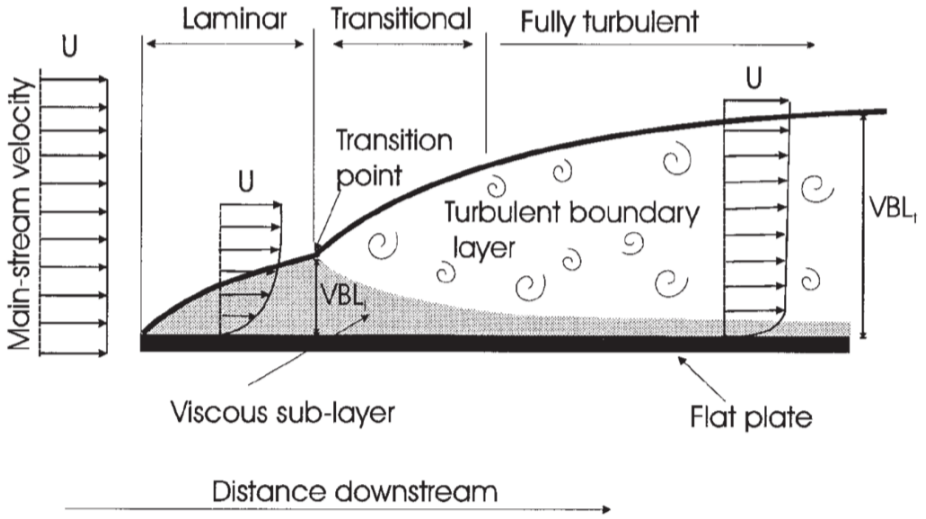

Figure 1.6: Schematic visualisation of the boundary layer and velocity profiles in x-direction along a smooth flat plate (Hurd, 2000).

Nepf (2012a) showed that the aquatic vegetation itself alters the mean and turbulent flow field. Two types of canopies were investigated; sparse submerged and dense submerged. In the case where the seagrass was placed sparsely together, bed roughness and near-bed turbulence was enhanced. The logarithmic velocity profile remained logarithmic. When the seagrass was put more densely together, the velocity profile was transformed to a mixing layer form. This suggests that the two cases generate two distinct types of turbulence; canopy-scale turbulence by flow instability at the top of the aquatic plant and stem-scale turbulence within the plant itself.

When studying the interaction with aquatic plants three aspects are important to investigate, namely flow interactions, drag forces and scaling issues. The area of hydrodynamics on aquatic vegetation is not highly investigated, but a collection of theoretical research papers have been written lately. Nikora et al. (2010) have investigated these aspects and developed a collection of similarity ratio to describe the physical interactions between flow and organism. The paper also promotes a new area of research called *Hydrodynamics of Aquatic Ecosystems*.

In the findings of Luhar and Nepf (2011) a theoretical model is developed to calculate the reconfiguration and drag forces of different types of aquatic plants. Another approach in trying to find the drag force and reconfiguration of flexible vegetation has also been developed by Whittaker et al. (2015). This model uses the vegetative Cauchy number to incorporate the effects of flexibility into the classical drag equation. The model will not be investigated further in this study. Scaling issues are investigated by Thomas et al. (2014), and focuses mostly on knowledge gaps existing today. The main idea presented is that there exists no knowledge if a scaled surrogate model represents the actual forces and motions occuring on a full scale plant in fluid flow.

1.3 Objectives

The main objective in this master thesis was to investigate the interaction between aquatic biological systems and their physical environments experimentally. The purpose of this study is to provide information on the plant-flow interactions and gain experimental knowledge of such interactions. Hence, to learn more about aquatic plant biomechanics in relation with engineering hydrodynamics. This thesis is a continuation of the work carried out in the project thesis delivered in Fall 2016 and the work of (Henry, 2016).

Intermediate objectives are listed below:

1. Give a literature review of flow and aquatic vegetation interactions.
2. Give the theoretical background for the vegetation-flow interaction, the hydrodynamic forces and scaling issues.
3. Perform, present and discuss results from preliminary flow experiments in the flume in order to map the flow conditions to be used in the final vegetation-flow interaction test.
4. Perform, present and discuss results from final vegetation-flow interaction experiments.

1.3.1 Limitations

Limitations in this master thesis are linked to three main categories:

- Laboratory facility
- Time
- Equipment

The laboratory facilities used are outdated, and gives limitations regarding flow control. For example, the flume tank does not have top of the line measuring equipment regarding velocity adjustment and other important features. Therefore, the experimental work rely on human resources and manual testing in order to map the flow conditions.

The time when doing a master thesis is limited, so only model testing with three different surrogates were performed in the time frame given. Therefore, further research is necessary to confirm the results given in this thesis. Linear theory is applied, but in some cases secondary effects may occurs in the results, and reasons for this observation is explained accordingly.

All the experiments are performed manually with first time experience in doing experimental laboratory work, which can lead to errors. In experimental testing of structures in fluid flow of a confined space, such as a flume, one can be affected by blockage effects from the structure affecting the flow. In this case the plant structure is slim, so the blockage effects are likely negligible.

1.4 Outline of the thesis

Chapter 2 gives a review of the hydrodynamic forces, biomechanics of aquatic vegetation, flow characteristics of open-channel flow and scaling issues.

Chapter 3 describes the preliminary flume analysis performed prior to the final testing of the plant models. Velocity tests, flume bed measurements, head loss and water elevation tests are presented. At last the process of making the surrogate models is explained. Turbulent Reynolds shear stresses are also investigated.

Chapter 4 describes the model tests performed in the flume regarding experimental set-up, data analysis and processing of the results.

Chapter 5 presents the results and discussions of the plant model behaviour, frequencies and drag forces of the final experiments.

Chapter 6 gives the conclusion of this master thesis and recommendations for further work.

Chapter 2

Theory

The following sections presents complementing theory in order to understand the behaviour, hydrodynamic forces and flow-interactions affecting aquatic vegetation. Hence, the first sections will explain the dominating hydrodynamic forces, and how these forces affect the biomechanics of the flexible organic structures. The last sections will investigate the theory of open channel flow and how turbulent processes can influence the plant motions. Lastly, scaling issues will be explained.

2.1 Hydrodynamics of vegetated flow

Ecosystems need a provider of nutrient to be sustainable. Aquatic vegetation functions as this provider, increasing the uptake of nutrients and production of oxygen (Nepf, 2012b). In some areas wide spread planting have been suggested because of the removal of nitrogen and phosphorous. The vegetation also creates a food web for marine life and promotes biodiversity. Lastly, these plants can also reduce coastal erosion and wave damping. All these services are in some way influenced by the flow field existing around and within the vegetated region. These advantages in aquatic ecosystems supports the need to investigate these processes further, as they can give increased knowledge on the resources found in the oceans.

2.1.1 Drag forces

Drag forces on aquatic vegetation has been of particular interest, because it has important engineering and ecological implications (Luhar and Nepf, 2013). Plant posture is controlled by drag at blade scale. This can influence the exchange of nutrients, oxygen and light uptake. Even stem rupture can happen if the drag forces get to excessive. As mentioned before, many

of the complex aspects around aquatic vegetation have not been investigated yet, and are only gaining popularity the past decade. Reconfiguration of flexible aquatic vegetation in flow is one of the aspects that have been investigated.

The relation of fluid drag to flow speed for flexible organic structures is important when studying plant-flow interactions. From this relation a reduction in the drag force is found due to body reconfiguration with increasing flow speeds (Alben et al., 2004). Reconfiguration is how the plant changes interacting with the fluid forces, and can be separated into two types, static and dynamic (Albayrak et al., 2014). Static reconfiguration is when waviness and flutter is not involved and one looks at the change of the plant shape in response to the changing velocity. Dynamic reconfiguration results from non-linear interactions, which leads to flutter or traveling waves changing the plant shape constantly. To understand the morphology of submerged plants withstand to large fluid forces serves as an important organising principle. For example, it is shown that the length and shape of seaweeds vary with different flow speeds experienced in its habitats (Alben et al., 2004).

The drag force is usually parametrised as (Henry, 2016),

$$F_D = \frac{1}{2}\rho C_D A U^2 \tag{2.1}$$

where ρ is the fluid density, C_D the drag coefficient, A the reference area of the plant, and U the uniform flow. When investigating a submerged rigid bluff body the drag force is proportional to the flow velocity squared. This yields for sufficiently high Reynolds numbers, *Re*. The Reynolds number is defined as $Rn = UD/\nu$, where ν is the kinematic viscosity and D is the characteristic length of the object. The Reynolds number is a ratio of inertial forces to viscous forces. Theoretical computation of pressure and viscous drag are usually a difficult process, the exception is for simple shaped bodies (Henry, 2016). For flexible and more complex shaped bodies, measurements must be relied on in order to find the drag force and parametrise C_D.

Friction and pressure drag

There exists two types of drag subjected from the flow on submerged bodies, friction and pressure drag (Çengel et al., 2010). Friction drag is caused by wall shear stresses τ_w, and

pressure drag, also called form drag, is caused by the pressure and is strongly dependent on the shape of the body affected by the forces. Bodies with a larger surface area experience more friction drag. Pressure drag is dominant mostly for blunt bodies, because it depends on frontal area of the body. For streamlined bodies the pressure drag is small.

The friction and pressure drag coefficient are as follows

$$C_{D,friction} = \frac{F_{D,friction}}{\frac{1}{2}\rho U^2 A} \tag{2.2}$$

$$C_{D,pressure} = \frac{F_{D,pressure}}{\frac{1}{2}\rho U^2 A} \tag{2.3}$$

Reducing drag by streamlining

A body subjected to drag forces from fluid flow will always try to streamline in the flow in order to minimise drag by reducing flow separation, thus reducing pressure drag (Çengel et al., 2010). In plant-flow interactions this defence mechanism is called reconfiguration.

Luhar and Nepf (2011) found a theoretical model to describe the flow-induced reconfiguration of flexible and buoyant blades of seagrass in fluid flow (Luhar and Nepf, 2011). The model is developed for individual blades that have the rectangular cross section characteristics of seagrass. They have shown that this mathematical model is able to predict drag and posture of other systems such as marine macroalgae with complex morphology.

One should be aware that assumptions are made in the theoretical model. Viscous skin friction is neglected. The blade of the seaweed is modelled as an isolated, buoyant and inextensible elastic beam. The beam has a constant width b, thickness t, elastic modulus E and density ρ_v. Figure 2.1 presents the coordinate system and force balance used in the theoretical model to derive mathematically the flow-induced reconfiguration of aquatic vegetation. For this entire section the relevant research from Luhar and Nepf (2011) are presented.

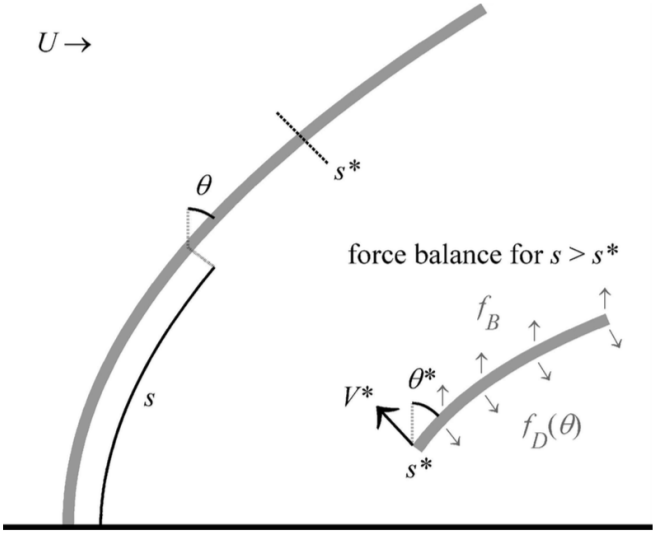

Figure 2.1: Flow-induced reconfiguration (Luhar and Nepf, 2011).

where U is the horizontal velocity that is uniform over the depth, θ the local bending angle relative to the vertical position where $\theta = 0$, s is the blade length where $s = l$ represents the tip of the blade, f_B the vertical buoyancy force, V the blade-normal restoring force due to stiffness and f_D the drag force. When the variables are presented with a star (*), it represents the forces happening at an arbitrary position s^* on the plant.

The drag force represented in this case is the form drag, and is derived from the velocity normal to the blade surface.

$$f_D = \frac{1}{2}\rho C_D b U^2 cos^2\theta \tag{2.4}$$

In this theoretical model it is assumed that the flow is steady and that the dominant hydrodynamic force is form drag. Form drag is the drag force due to the irregularity of the shape of the body that interacts with the fluid flow it is moving in. To reduce this type of drag the body uses reconfiguration. In the reconfiguration two different mechanisms works to reduce the drag. The first, is reducing the frontal area of the plant, and the second is streamlining. From the research Luhar and Nepf (2011) have done on the topic of flexible plants a physically motivated empirical relationship of effective length is suggested.

$$\frac{l_e}{l} = 1 - \frac{(1 - 0.9C_a^{-1/3})}{1 + C_a^{-3/2}(8 + B^{3/2})} \tag{2.5}$$

where l_e is an effective length they introduce, so that the characteristic area becomes $A = bl_e$, where b is the characteristic width. C_a is the Cauchy number. B is the buoyancy force, and l the blade length. The advantage of this model is that it can account for two distinct physical phenomena that can affect the drag. These are the Reynolds number and the reconfiguration. The Reynolds number is accounted for through the drag coefficient, C_D, and the reconfiguration can be accounted for through the effective length that is governed by the Cauchy number, C_a, and the buoyancy parameter, B. To estimate drag one would use

$$F_{x0} = \frac{1}{2}\rho C_D b l_e U^2 \tag{2.6}$$

where the drag coefficient, C_D, for an rigid, upright blade would be used.

The Cauchy number as mentioned does play an important role in predicting drag and reconfiguration of flexible plants as seen from the previous theory and calculations. It quantifies the objects flexibility when exposed to a fluid flow by a ratio between the elastic and inertial forces (Whittaker et al., 2015).

$$C_a = \frac{\rho U^2 A_p H^2}{EI} \tag{2.7}$$

where A_p is the frontal projected area, ρ is the water density, U is the horizontal velocity, and H is the height of the vegetation. EI is the flexural rigidity.

2.1.2 Vortex-induced vibrations

A flexible plant stem submerged in water can in many cases be compared to circular cylinder exposed to fluid flow. Flow around a fixed circular cylinder is affected by many parameters, such as Reynolds number, free stream turbulence and surface roughness among others (Bearman, 2011). Among these parameters vortex-induced vibrations play an important role in the plant behaviour. Although, it is not yet demonstrated, flexible cylinders, such as a plant stem, can likely be sensitive to the same parameter responses. However, the investigation of vortex-induced vibrations on flexible structures face many challenges as it is complex processes that have yet to be investigated. In this section the focus will lay in the basic building blocks of VIV on circular cylinders in comparison to flexible plant stems.

One of the main factor characterising the fluid flow is the Reynolds number (Faltinsen, 1980).

$$R_n = \frac{UD}{\nu} \tag{2.8}$$

where U is the characteristic free-stream velocity, D is the characteristic length of the body and ν is the kinematic viscosity coefficient. The Reynolds number is important in order to determine if the fluid flow around an organism is laminar or turbulent. This knowledge give information on mass and momentum transport, which is dependent on these properties (Hurd, 2000). Other factors that influence the flow around a circular cylinder are free-surface effects, body form, sea floor effects and reduced velocity, especially for an elastically mounted cylinders with natural frequency f_n.

Potential theory

The external flow around bodies can be treated as inviscid and irrotational, because the viscous effects are limited to a thin layer next to the body called the boundary layer (Pettersen, 2007). Boundary layer theory will be explained in Section 2.3.1. Potential theory is used to simplify calculations regarding fluid flow past a circular cylinder. The potential theory creates a foundation for the linear theory used in this thesis.

When investigating potential theory in steady uniform flow past a fixed circular cylinder tangential velocity past the cylinder becomes

$$U_e = 2U_\infty \sin(\theta) \tag{2.9}$$

where U_∞ is the incident flow velocity and θ is the angular coordinate ($\theta = 0$ corresponds to the forward stagnation point). From Bernoulli's equation the pressure on the body is defined as

$$p + \frac{1}{2}\rho U_e^2 = p_0 + \frac{\rho}{2}{U_\infty}^2 \tag{2.10}$$

where p_0 is the ambient pressure. The resulting pressure coefficient can be written as

$$C_p = \frac{p - p_0}{\frac{1}{2}U_\infty^2} = 1 - 4\sin^2(\theta) \tag{2.11}$$

Vortex shedding

Although, in the inviscid theory like potential theory the tangential velocity can be written as equation 2.9. However, close to the body of the cylinder it is not valid (Faltinsen, 1980). In the boundary layer viscous forces are dominating. Therefore, in the fluid around a circular cylinder will in reality consist of instabilities that causes asymmetry and alternating shedding will occur from each side of the cylinder as in 2.2 (Faltinsen, 1980).

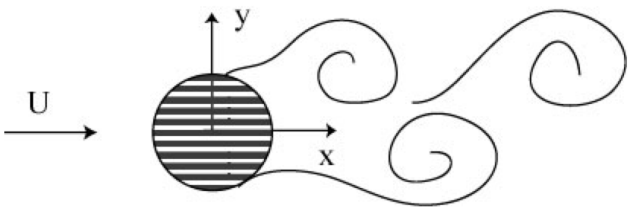

Figure 2.2: Classical vortex shedding around a circular cylinder(A.H. Techet, 2004).

The shear layer instability causes vortex roll-up in the wake, because the flow speed is much higher outside the wake than inside. This is caused by separation on the cylinder when the velocity and the Reynolds number increase. The vortex- shedding is dictated by the Strouhals number, as seen in equation 2.12.

$$St = \frac{f_v D}{U_\infty} \tag{2.12}$$

where f_v is the shedding frequency, D is the diameter and U is inflow velocity. The Strouhals number is approximately constant ($St = 0.2$) over a range of Reynolds numbers seen in Figure 2.3.

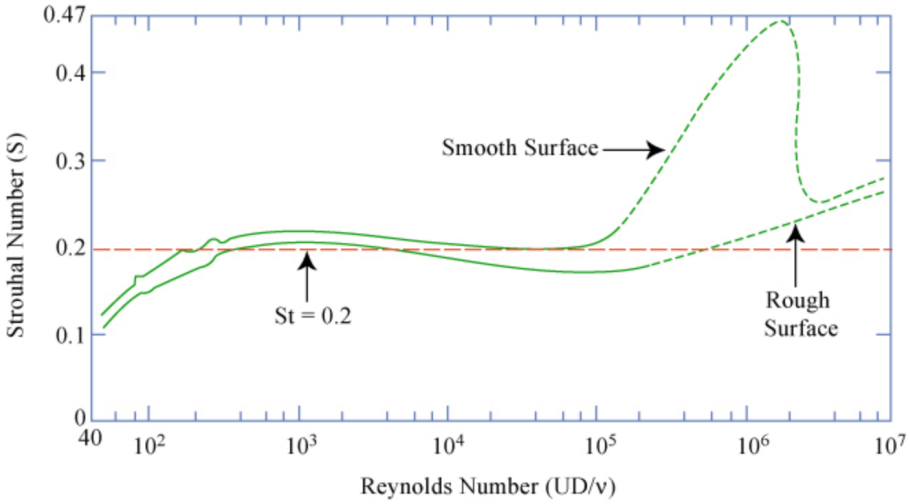

Figure 2.3: The relation between Strouhals number and Reynolds number over a circular cylinder (Flickr, 2017).

When a vortex sheds a opposite circulation occur around the cylinder, it creates an increase in the velocity on top (point A) of the cylinder, and a reduction at the bottom (point B). This results in the pressure at the bottom being higher than the pressure on the top as in Figure 2.4. The difference creates an upward lift force. The same process but opposite will happen when the next vortex sheds from the bottom of the cylinder. The drag force will also oscillate because of the vortex shedding, and is approximately 10-20% of the mean value of the drag force. The drag force has the same direction independent of the vortex shedding. The drag force oscillates with twice the frequency of the lift (Faltinsen, 1980). The equations are written as equation 2.13 and 2.14.

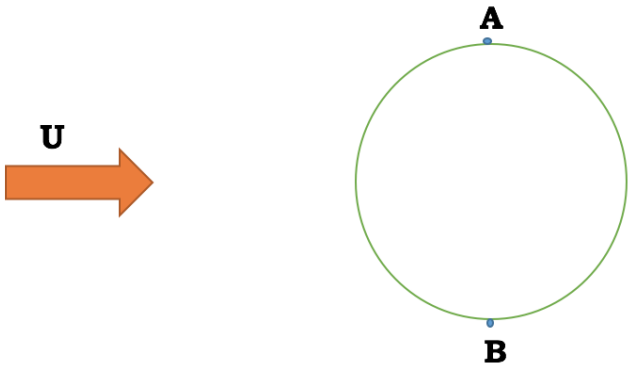

Figure 2.4: A circular cylinder with an uniform inflow velocity U with point A at the top and point B at the bottom.

$$C_L = \frac{F_L}{\frac{1}{2}\rho A U^2} \tag{2.13}$$

$$C_D = \frac{F_D}{\frac{1}{2}\rho A U^2} \tag{2.14}$$

Lock-in

Lock-in is the phenomenon occurring when the the vortex shedding and the structural vibration frequencies coincide (Pettersen, 2007). When lock-in occurs the largest amplitude oscillations take place, and can cause harm to the cylinder or in this case, the plant stem.

$$\omega_v = 2\pi f_v = 2\pi S_t(\frac{U}{d}) \tag{2.15}$$

where ω_v is the shedding frequency.

$$\omega_n = \sqrt{\frac{k}{m + m_a}} \tag{2.16}$$

where ω_n is the natural frequency of oscillation, k is the stiffness, m is the mass and m_a is the added mass term.

2.2 Biomechanics

Physical forces caused by fluid flow makes organisms react in different ways. These motions are highly dependent on the biomechanical properties of the organism (Nikora et al., 2010). This following section uses the findings of Nikora et al. (2010) to explain this phenomenon. The biomechanics are important in order to understand plant-flow interactions, but in this thesis the focus will lie in the field of hydrodynamics. A brief introduction to biomechanics of submerged aquatic plants is presented here.

Morphology is defined as the form and structure of an organism. Examples of morphologic characteristics are linear, volumetric, areal and density as illustrated in Figure 2.5. These

properties define how flow-plant interactions will affect the behaviour of the plant, especially regarding drag forces.

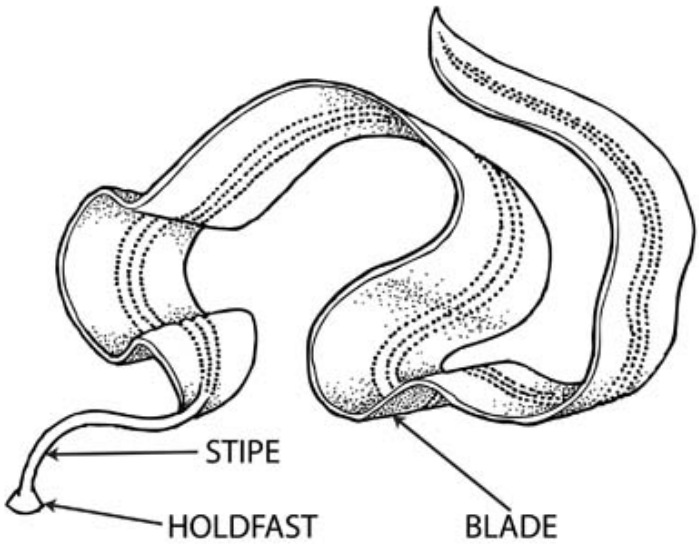

Figure 2.5: Morphological structure of the kelp *Cymathere triplicata* (Dingeldein, 2009).

Material characteristics defines how the material the organism consists of affects behaviour. Examples are material density, Young's modulus, flexural stiffness and second moment of cross-sectional area. Material properties can influence the aquatic plants flow interaction, and is also an aspect that can defines how the plant behaves.

Flow interaction characteristics are the different parameters used to quantify the interplay with plants and flow such as drag and lift coefficients, bending moments, strain and tension forces. These are the most important aspects in a hydrodynamic sense.

To properly show the coupling between the hydrodynamic environment and the submerged plant hydrodynamic interactions are investigated. These interactions consists of a set of forces, and the ratios between them. These ratios explain how they interact with each other. The following set of forces are the main influencers in plant-flow interactions:

Flow-induced forces

$$F_D = \frac{1}{2}\rho C_D U^2 A \tag{2.17}$$

$$F_L = \frac{1}{2}\rho C_L U^2 A \tag{2.18}$$

where F_D are the drag forces and F_L the lift forces. ρ is the densities of the fluid, U is the velocity of the free stream A is the plant area.

Plant-induced forces

$$F_B = \rho g V_p \tag{2.19}$$

$$F_G = \rho_p g V_p \tag{2.20}$$

where F_B the buoyancy forces and F_G the gravity forces. ρ_p is the density of the plant, g is the gravity acceleration, and V_p is the volume of the plant.

Plant-reaction forces

$$F_T = E\epsilon A \tag{2.21}$$

$$F_b = \frac{EI_2}{R\lambda} \tag{2.22}$$

F_T the tensile (reaction) forces and F_b are the bending (reaction) forces. ϵ is the strain (relative elongation) imposed by the fluid, λ is the distance from the bed surface to the point where the fluid resultant force acts, R is the radius of curvature at a point where a bending force is defined, E is the Young's modulus and I_2 is the second moment of area of the plant.

When utilising these forces and their ratios, similarity numbers can be deduced. These can be used to study and model organism-flow interactions. The ratios are as follows:

$$\frac{F_B}{F_G} = \frac{\rho g V_p}{\rho_p g V_p} \qquad \Rightarrow \qquad \mu_{B-G}\frac{\rho}{\rho_p} \tag{2.23}$$

$$\frac{F_D}{F_G - F_B} = \frac{\frac{1}{2}\rho C_D U^2 A}{(\rho_p - \rho) g V_p} = \frac{\rho}{(\rho_p - \rho)} \frac{\frac{1}{2}\rho C_D U^2 L d}{g L d^2} \qquad \Rightarrow \qquad \mu_{D-B} = C_D \frac{\rho}{(\rho_p - \rho)} \frac{U^2}{g d} \tag{2.24}$$

$$\frac{F_D}{F_b} = \frac{\frac{1}{2}\rho C_D U^2 AR\lambda}{EI_2} \qquad \Rightarrow \qquad \mu_{D-b} = C_D \frac{\rho U^2}{E}\left(\frac{L}{d}\right)^2 \tag{2.25}$$

where d is the small plant scale, for example the stem diamter, and L is the large plant scale, such as shoot length.

From these calculations three similarity numbers emerge. μ_{B-G} and μ_{D-B} have both been used in previous studies and modeling of aquatic vegetation with desired results. The studies focused on mass-transfer processes in communities of benthic periphyton (organisms that live on the surface of submerged objects like plants and other underwater bodies), and organism-flow interactions. All of the similarity numbers tell something important about the interactions between organisms and flow, however, the similarity number μ_{D-b} is one of extra interest to this project.

μ_{D-b} can distinguish between two types of aquatic plant body interactions, the "tensile" and the "bending" plant. An example of this plant behaviour is illustrated in Figure 2.6. For "tensile" plants the similarity number is large, and for "bending" plants small. The plant with "tensile" behaviour will experience mostly viscous drag and tension forces. This is due to the low flexural rigidity, and makes the plant follow the flow passively. On the other hand, the "bending" plant will have high flexural rigidity and experience pressure drag due to vortices created by the downstream flow on the plant. The plant will also experience bending forces due to the rigidity, and withstanding the forces of the fluid flow.

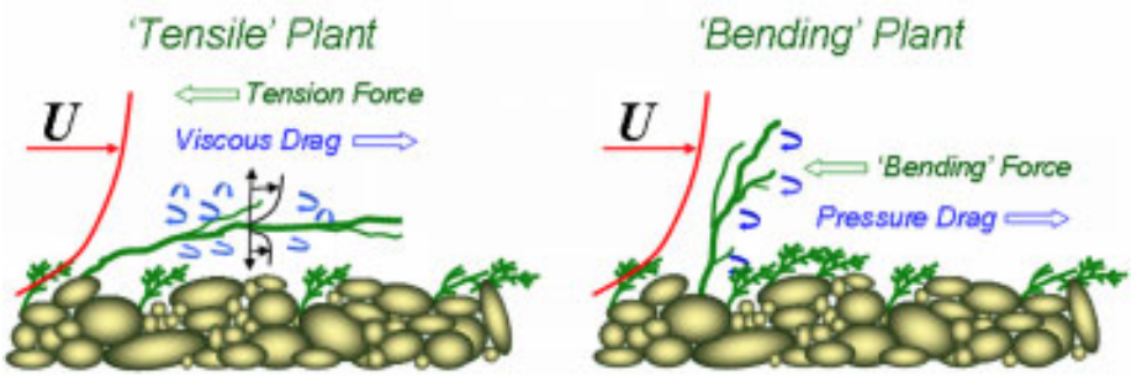

Figure 2.6: **Two types of plants in flow:** The tensile plant has low flexural rigidity and passively follows the flow and experience mostly viscous drag. The bending plant has high flexural rigidity and it resists the flow more. This creates downstream vortices and pressure drag (Nikora et al., 2010).

2.3 Open-channel flow

Open-channel flows can in many ways be compared to flows through pipes, or a rectangular duct (Çengel et al., 2010). An example is a conduit that is not completely filled with water, thus it has a free surface. A steady uniform flow in a straight channel can be a simplification of flows in the natural world (Prof. John Southard, 2006). This concept can be transferred to the fluid flow in a flume tank. In an open channel the velocity is zero at the bottom and sides, because of the non-slip condition. The velocity is at maximum at the mid-plane of the flow (Çengel et al., 2010). The following section presents the theory behind open-channel flow.

2.3.1 Boundary layer theory

In many cases fluid flows with low viscosity and high Reynolds numbers may be a good approximation, but one important aspect is not considered in this theory (Schlichting and Gersten, 2017). In this situation the no-slip condition is not satisfied. The no-slip condition takes care of the transition at a thin layer close to the wall, where the velocity is retarded and comes to zero at the wall. This implies that the flow field can be divided into two regions, one in the bulk of the flow region where the viscosity can be neglected, and one close to a wall boundary where viscosity is important.

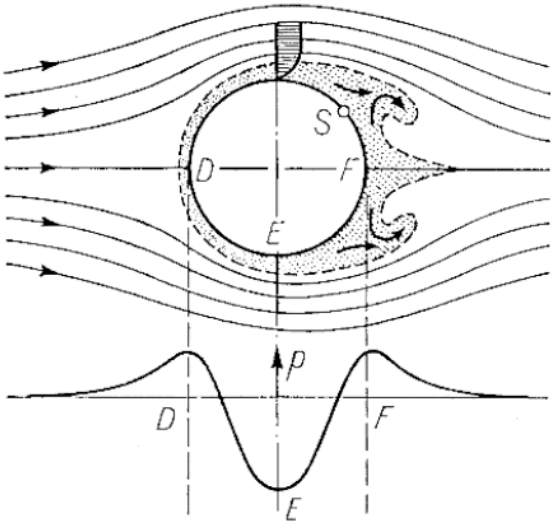

Figure 2.7: Separation of the boundary layer, and vortex formation on a circular cylinder (Schlichting and Gersten, 2017).

In Figure 2.7 the boundary layer around a circular cylinder is presented. Here, the boundary layer creates a separation, which causes vortices to shed behind the cylinder. This effect creates lift and drag forces affecting the cylinder in the flow. When the velocity of the flow increases vortices starts to appear in the viscous sublayer, as seen in Figure 2.8. At high velocities the vortices will create turbulent flow. This happen for Reynolds numbers higher than approximately 2300. In a flume tank wall effects can also occur, because of the viscous sublayer across the walls with the no-slip condition at the wall. This effects can create disturbances affecting the body in the flow.

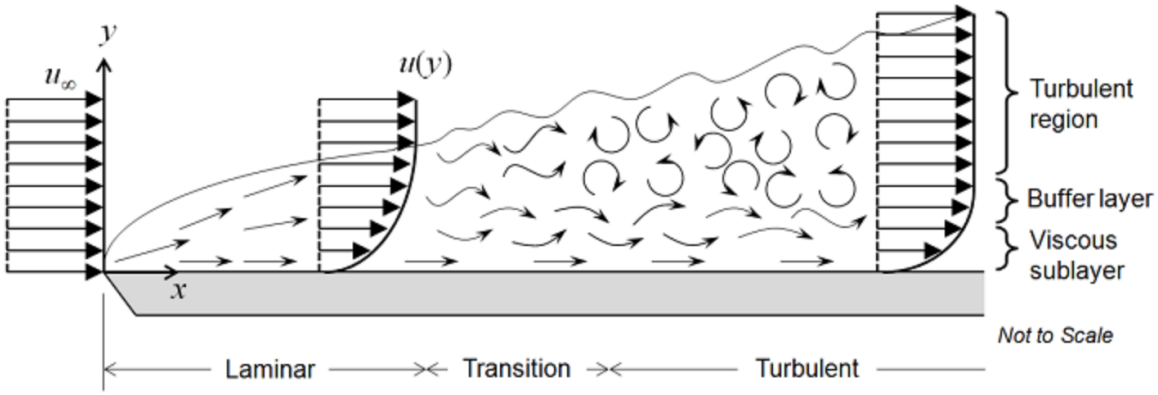

Figure 2.8: The transition occurring for increasing velocities with the boundary layer close to the bed (Comsol, 2017).

2.3.2 Turbulent flow

First of all, most fluids encountered in real life are turbulent. When observing a fluid in a flume tank the wall shear stresses can be affected by turbulence (Çengel et al., 2010). Turbulent flow is immensely complex and dominated by fluctuations. To this day researchers have not fully understood this phenomenon. Hence, relying on experiments and empirical correlations found through these tests.

When a flow is turbulent it is characterised by rapid fluctuations in a disorderly manner. Regions of the fluid create swirling motions, also called eddies. Mechanisms for momentum and energy transfer are produced in these fluctuations. In comparison to laminar flow which has fluid particles flowing in streamlines where energy and momentum are transferred across these lines by molecular diffusion. In contrast, turbulent flow can transfer en-

ergy, momentum and mass much faster than laminar flow with molecular diffusion. This is why turbulent flow inhibits higher values of friction, mass and heat transfer coefficients.

When the flow investigated is steady there still exists turbulence in the form of eddy motions that cause fluctuations (Çengel et al., 2010). These fluctuations influence the values of velocity, temperature and pressure, and makes them vary across the flow. In this thesis velocity is the only component of interest. The instantaneous values of velocity will fluctuate around an average value and with time. The velocity is then expressed as a sum of an average value ($\bar{u}$) and a fluctuating component (u'):

$$u = \bar{u} + u' \tag{2.26}$$

The average value of the fluctuating velocity at a given location is determined by averaging over time. The time interval needs to be sufficiently large. This means that the time average interval will move towards a constant. The time average of the fluctuating components will then be zero as a consequence of this.

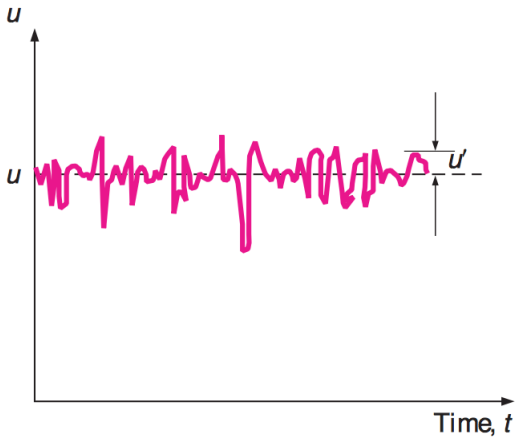

Figure 2.9: Fluctuations of the velocity component u (Çengel et al., 2010).

Eddies happening in fluid flow have a high frequency making them effective for the transport of momentum, thermal energy and mass, even though the magnitude of u' is only a small percentage of $\bar{u}$. A dominant role in pressure drop is the chaotic fluctuations of the fluid particles, so these fluctuating particles must be considered in analysis with the mean velocity.

The turbulent velocity profiles in vertical and cross-sectional direction are based on both

measurement and analysis compared to the laminar ones (Çengel et al., 2010). They are thus determined from experimental data, and are semi-empirical in nature. A comparison of the cross-sectional and vertical velocity profiles are shown in Figure 2.10.

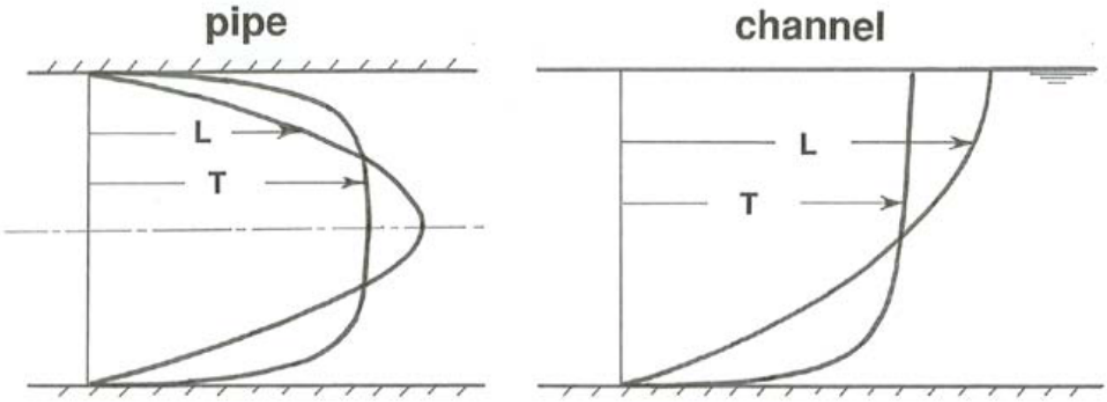

Figure 2.10: Comparison of laminar and turbulent velocity profiles in uniform steady flow for a pipe and an open-channel flow (Prof. John Southard, 2006)

Turbulent flow along a wall has four regions, viscous sublayer, buffer layer, inertial sublayer and outer layer, as seen in Figure 2.11. This origins from the boundary layer theory, and displays the divisions of the turbulent flow from viscosity dominated to turbulence dominated.

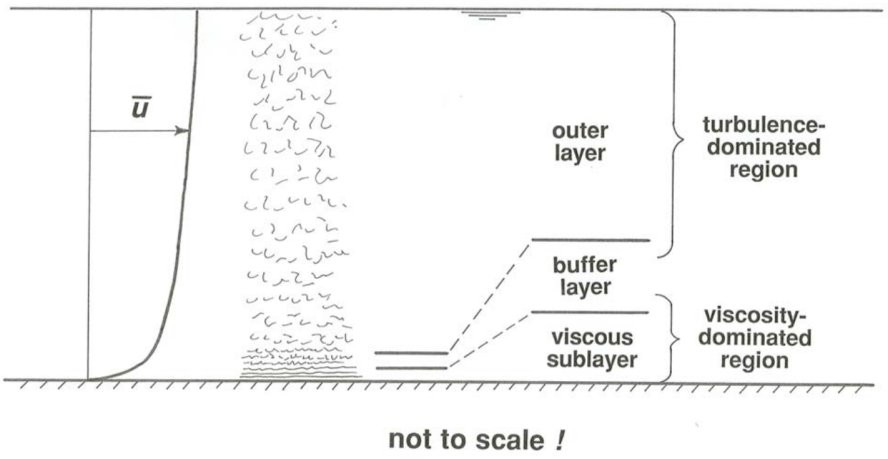

Figure 2.11: The four layers of the turbulent flow across a fixed wall in open-channel flow (Prof. John Southard, 2006).

Reynolds stresses

The Reynolds stresses or turbulent shear stresses are the mean forces per unit area imposed on the mean flow by fluctuations (Prof. John Southard, 2006). The forces are calculated by Reynold averaging the Navier-Stokes equations, and the general form of the Reynolds stress tensor is written as

$$\tau_{turb} = -\rho\overline{u'v'} \tag{2.27}$$

where $\overline{u'v'}$ is the time average of the product of the fluctuating velocity u' and v' (Çengel et al., 2010).

In the boundary layer of the turbulent flow, the velocity varies vertically. These variations in the velocities will cause a shear stress in the flow, the Reynolds stress. The shear stress varies over the depth as shown in Figure 2.12.

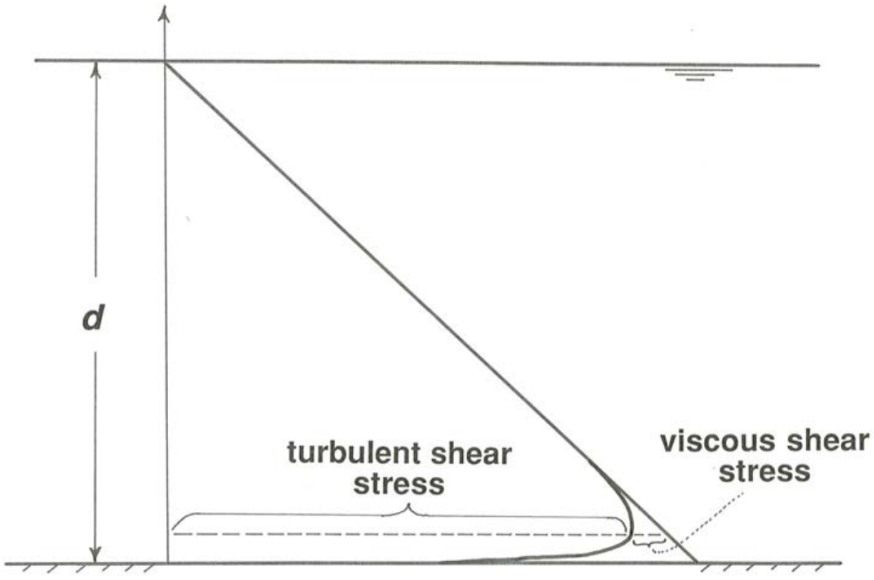

Figure 2.12: The distribution of the total shear stress, turbulent shear stress and viscous shear stress in a steady uniform flow in an open-channel (Prof. John Southard, 2006).

2.4 Scaling issues

This section investigates the issues of scaling aquatic vegetation. In this master thesis this topic is presented with a brief overview of the issues regarding scaling submerged aquatic plants. The surrogate models in the model tests are in a different scale than the actual plant, *Laminaria Digitata*, which is approximately 2 m high in its natural habitat. A question to ask is whether the behaviour and forces acting on the model will replicate the real world (Thomas et al., 2014). Scaling of aquatic plants depends on aspects that can be measured both experimentally and in field work in natural environments. When scaling models of aquatic plants today Froude or Reynolds scaling are used as a basis of comparison, but the scaling of the biological factors have not been considered. This gives knowledge gaps in the research. The problem of scaling arise when the parameters do not scale linearly. Another problem is quantities that are hard to envision how to scale. For example, when wanting to scale population density of living aquatic vegetation, how do you scale competition between the plants? There has not been carried out enough research on this topic yet, especially on full-scale tests in laboratories with real living plants. Therefore, it is beneficial to do research on the topic of scaling, especially the biological aspects, to find if the surrogate model reflects the actual behaviour of the plant.

Steen et al. (2014) presents similarity requirement that needs to be fulfilled when scaling from full scale to model scale. The three requirements are:

Geometric similarity is given if the full scale and model scale has the same shape.

Kinematic similarity is achieved if the ratios of the velocity in model and full scale are equal.

Dynamic similarity is obtained if the ratios between all the forces that contribute in both full and model scale are to be constant.

In this case the surrogate model represents the model scale and the kelp *Laminaria Digitata* represents the full scale. The surrogate model is a simplified shape, and for this reason one can not fully know if the behaviour of the model in incoming flow will represent the real plant as it has a more complex shape. The variations of the velocities in the habitat of the kelp is hard to determine, and needs more research before the flow field can be mapped properly. Therefore, the flow field around the model of the kelp will be a simplified version, but the in-

formation gained from the flow experiments is likely to increase the general knowledge of the plant-flow behaviour. Dynamic similarity is difficult to achieve as this is complex processes with many factors influencing the system. For this reason scaling issues are only addressed in this thesis. Further research is necessary in order to capture the complexity of the scaling of aquatic plants.

Chapter 3

Flume characteristics analysis

Submerged bodies are usually tested in flumes to measure important parameters in the flow affecting the structure. An example of these parameters are hydrodynamic drag forces (Cooper et al., 2007). Flumes provide control of a number of parameters as flow velocity and flow depth. Flume width, reconfiguration, initial set-up of flexible bodies and other details of the flume design plays a crucial role in force measurements. In order to map the flow behaviour in the flume a series of tests are necessary. The flume used for testing in this master thesis is outdated regarding instrumentation, and therefore needs even more pre-testing. Prior to the final model tests flow measurements were measured in order to find head loss, velocities and inaccuracies in the flume bed and water elevation. In the following sections preliminary tests are presented to analyse the characteristics of the flow field in the flume. Five tests were performed during the preliminary testing. The tests were carried out in Spring 2017. All the tests were performed in the same flume tank over a range of velocities. Four of the tests were performed before the velocity profile measurements with Acoustic Doppler Velocimetry. One test were carried out after the ADV testing. In the following sections the flume properties, test set-up, test conditions and significant results are presented.

3.1 Flume properties

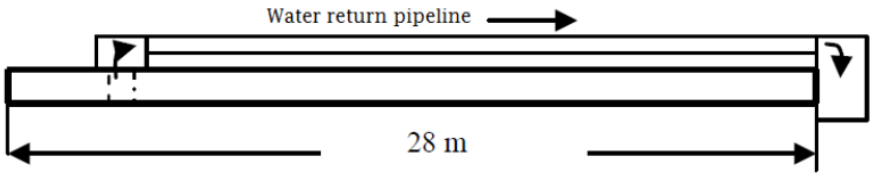

Figure 3.1: A simple sketch of the flume seen from above. Flume dimensions: 28 m long, 0.6 m wide and 0.4 m water depth (Henry et al., 2012)

.

Figure 3.2: The appearance of the flume tank at the Department of Hydraulic and Environmental Engineering at NTNU

The flume consists of sections with two materials, wood and glass. The glass walls are connected by a metal framework. The difference between the sections may have an impact on the preliminary and final measurements, as it likely makes uneven points along the bed of the flume tank. In the beginning of the semester the inlet conditions of the flume were improved by the technicians at NTNU. The previous inlet had proven to make the flow uneven and had a jet flow that is not ideal in a flume flow when performing testing. This was mapped in Fall 2016 in the project thesis by ADV testing measuring velocities. From the velocity profiles found a jet was observed, but due to the unideal flow conditions the measurements were considered weak. Therefore, the decision to change the inlet condition was made. A comparison with the old and new velocity profiles is presented in Section 3.3.3. A block with straight circular rods was put at the inlet to straighten the flow and restrict vortices from being created at the inlet. After the straightener a honeycomb filter was installed improving the flow even more. Styrofoam plates were also put at the inlet and outlet to diminish fluctuations in the fluid flow. A comparison of the old and new inlet condition is seen in Figure 3.3.

Figure 3.3: The old inlet condition and the new inlet condition. The far left shows the old inlet condition, the middle the new honeycomb, and to the far left the new inlet with the straightener.

.

3.2 Preliminary-tests

The following sections present the experimental tests performed in preparation for the final model tests on plant-flow interaction and drag forces. Information about instrumentation, experimental set-up and results are presented. All the experiments were performed in the flume tank utilised in the final tests. Therefore, the information gained from the preliminary tests will be utilised in analysing the final test results. The investigations will also help give vital knowledge on the flume conditions for future experiments. The coordinate system in the tank is as follows with origo set at the inlet (in front of the straightener) with x-direction in flow direction. Y-direction is set across the width of the tank and z-direction gives the depth in vertical direction. All the measurements started at point *423 cm* in x-direction, except the head loss test. The tests are prone to small changes in the rail where the measurement equipment are set-up caused by the outdated flume.

3.2.1 Simple velocity test

The flume has a system where the velocity of the flow is adjusted by a voltage switch. For this reason a simple velocity test was carried out to find what type of voltage represent the different velocities. The test was performed two separate times in order to make sure the same velocities were present in the flume at all times. The test was performed by using a

small object in cork material, and take the time it took to travel the distance of *13 m*. A range of voltages were tested, *8-45 V*, where *45 V* was the highest flow rate possible before the water went over the straightener at the inlet of the flume. The flow rate of *45 V* was removed due to the problem of flooding the straightener. The results are presented in Figure 3.4. The conversions are presented in Table 3.1. These five velocities are used for the rest of the preliminary tests and the final model tests.

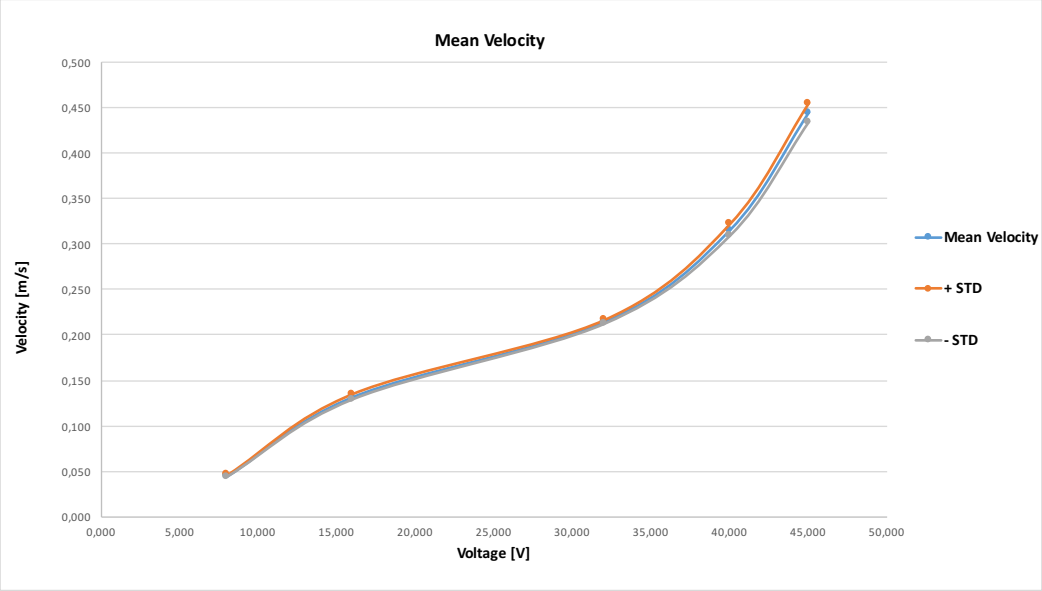

Figure 3.4: Mean velocities for different voltages.

Table 3.1: Mean velocities for a range of voltages used for further testing.

Mean Velocity	
Voltage [V]	**Velocity [m/s]**
8	0.05
16	0.14
24	0.17
32	0.21
40	0.34

3.2.2 Flume bed measurements

The fluid flow can be influenced by an uneven flume bed slope. Slope variations in the flow direction, and variations across the flume may affect the flow regime and influence experi-

ments in the flow (Henry, 2016). An uneven bed can create bed roughness, which may cause forming of vortices and second-order effects. Performing bed slope measurements by using two measurements points, the flume bed and free surface, as reference is only adequate in tests where the flow is steady and uniform over a smooth bed (Henry, 2016). These assumptions hold for this case where the flume bed is smooth with no sediments added as the bed.

In order to measure the bed a point gauge was used. The free surface was set as the zero level. The water depth was set to *40 cm* for the measurements in x-direction. All the measurements were carried in calm water. The first test measured the slope downstream in x-direction along the flume, and was carried out in the middle of the flume at *y=30 cm*. The measurements were performed for every meter from *423 cm* to *1400 cm*, and the points were measured five times in order to obtain more correct data sets and minimising human errors in the measurement technique. Measurements were also carried out in y-direction at the same points as in x-direction. The points measured were *10-50 cm* for every tenth centimetre across the width of the flume. The water level was lowered to *25 cm* for this test as the point gauge was not of adequate length to measure a zero-point at the free surface and still measure the change at the bed. This was the result of a different mount for the point gauge making cross measurements possible. A small change of width of the tank across the walls can also affect the fluid flow, for this reason a brief test was carried out. The simple measurements across the flume indicated no changes of significance and therefore the tank width is assumed to be *60 cm* across the flume.

The results showed a change both downward and across the flume. The maximal slope change occurred at point *923 cm* in x-direction with a change of approximately *8.5 mm*. The maximal change in y-direction occurred at point *1123 cm* and had a change of approximately *3 mm* from point *10 cm* to *50 cm*. Small changes in y-direction are occurring for all the points measured. From these results one should be aware that these changes may affect the flow in the final tests. The results is presented in Figure 3.5 and 3.6.

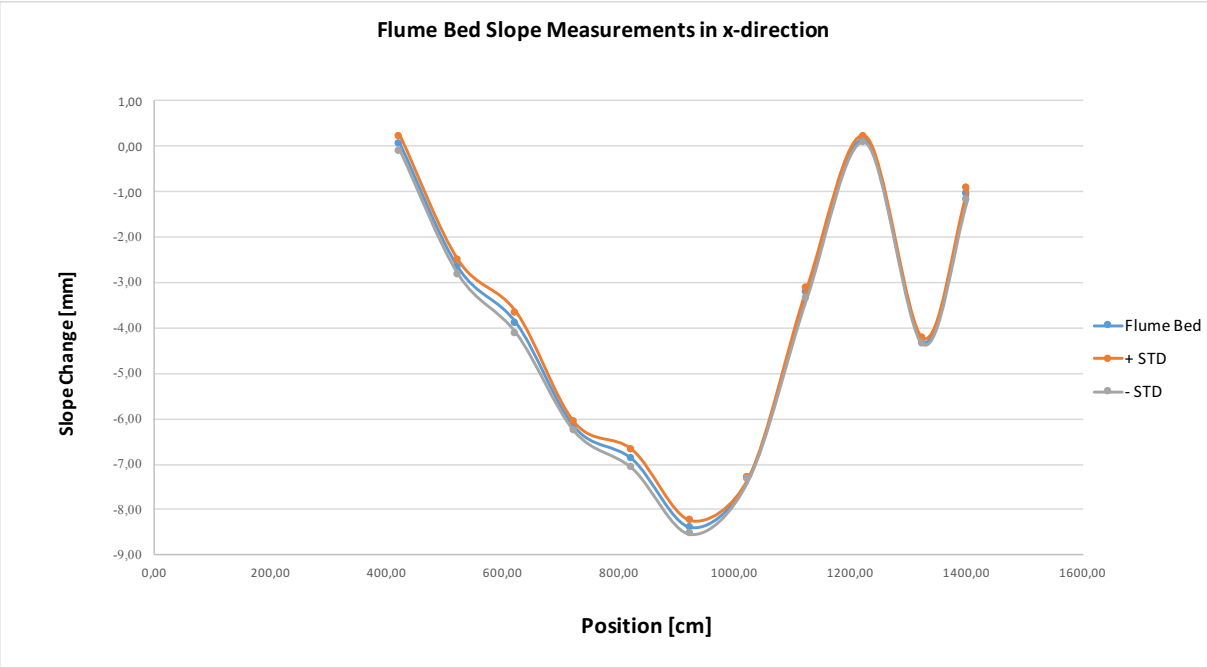

Figure 3.5: Flume bed slope variations in x-direction.

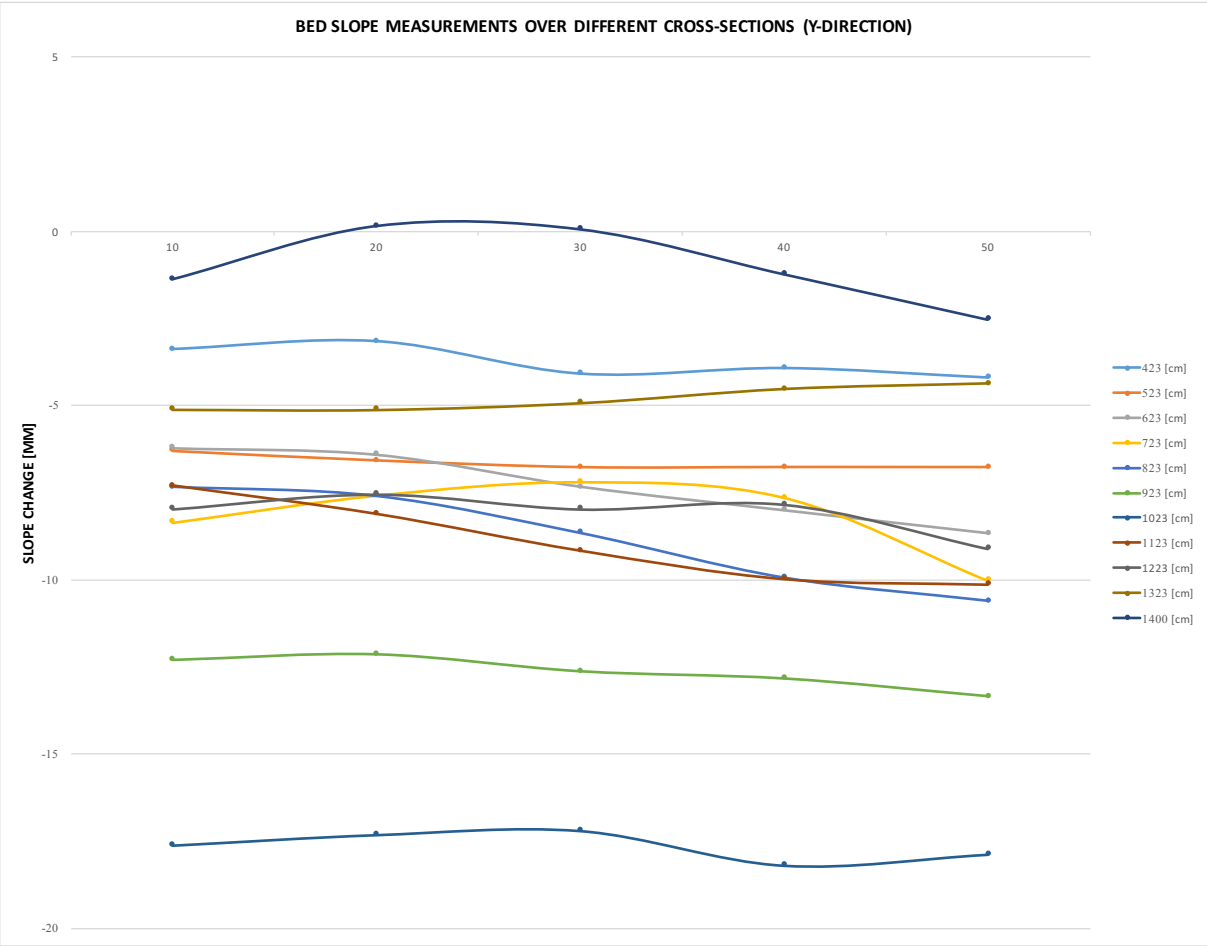

Figure 3.6: Flume bed slope variations in y-direction.

3.2.3 Water elevation test with varying water depth

The water elevation of the free surface may vary across the flume, and cause changes in the flow affected by bed changes and fluctuations at higher velocities. In this test the water depth was set to *40 cm* and when the velocity in the flume increases the water level will diminish along the flume length. This is caused by head loss originating from the inlet by the honeycomb and straightener braking the fluid flow. The water elevation tests were performed for the five velocities found in Section 3.2.1 at every meter from point *423 cm* to *1400 cm*. The measurements were carried out in the middle of the flume at *y=30 cm*. The different points were measured five times at each point. The results are presented in Figure 3.7, and implies the same changes observed at the flume bed affects the water elevation too. The free surface also started to fluctuate at the two highest velocites, *0.21 m/s* and *0.34 m/s*, which made the measurements prone to errors.

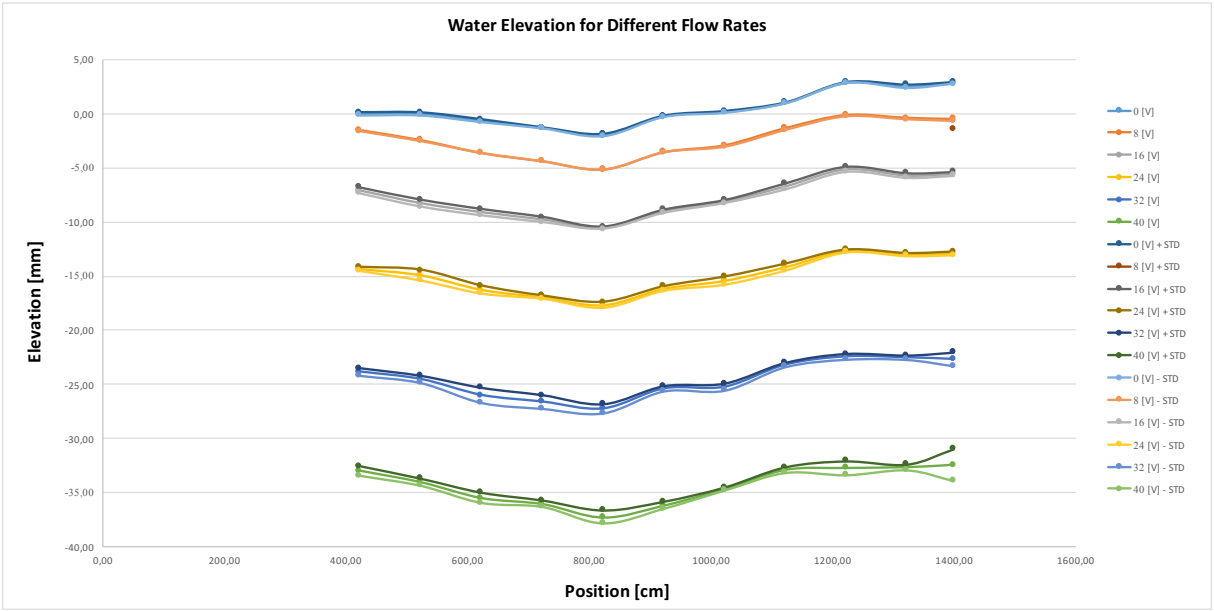

Figure 3.7: Water elevation with varying depth.

3.2.4 Water elevation with constant water depth

A test to measure the elevation of the free surface with constant depth was performed after the ADV measurements explained in Section 3.3. The test was carried out after, because it would be beneficial to compare the ADV results with the water elevation results to observe if they had any correlations. This will be commented in the result section of the ADV mea-

surements in Section 3.3.3. The test was performed in the same way as the water elevation test presented in Section 3.2.3. The water level was adjusted accordingly for every velocity in order to obtain the water level at *40 cm* throughout the entire experimental test. At the higher velocities, *0.21 m/s - 0.34 m/s* it was difficult to obtain a constant water depth because of fluctuation in the flume flow. From the results, as presented in Figure 3.8, one can observe that the elevation with constant water depth has the same variations and tendencies as the elevation with varying depth. This may support the observation that the flume bed slope changes affect the flow.

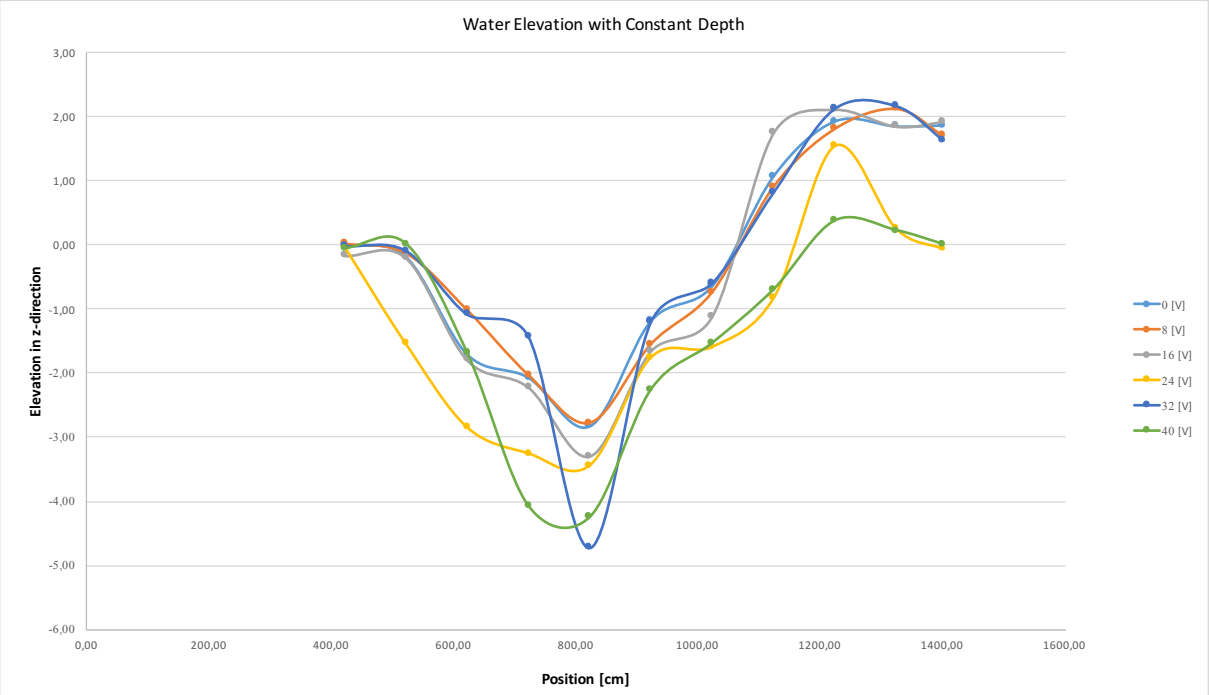

Figure 3.8: Water elevation with constant depth.

3.2.5 Head loss

A new inlet system is recently set-up in the flume with a honeycomb and a straightener previously explained in Section 3.1. The inlet creates head loss at the various velocities. The head loss was measured at different points in front, middle and behind the new inlet system as seen in Figure 3.9. As previously observed from the simple velocity test in Section 3.2.1 the flume has a velocity limit of *0.34 m/s* or else the water flow will flood the inlet condition. Thus, it gives a limit for the maximum velocity obtained in the flume with this inlet set-up. The energy loss created by the head loss sets this limit, since the straightener consists of

many pipes and the honeycomb of many small channels limiting the fluid flow. To omit this limitation an improvement to the inlet must be performed to have the possibility of testing higher velocities. In this thesis the limitation will not affect the final results. The results from the head loss analysis is presented in Figure 3.9. As shown in the results there exists a significant head loss because of how the inlet is designed. The head loss is also caused partly by the viscosity of the fluid and friction forces occurring naturally in the flow.

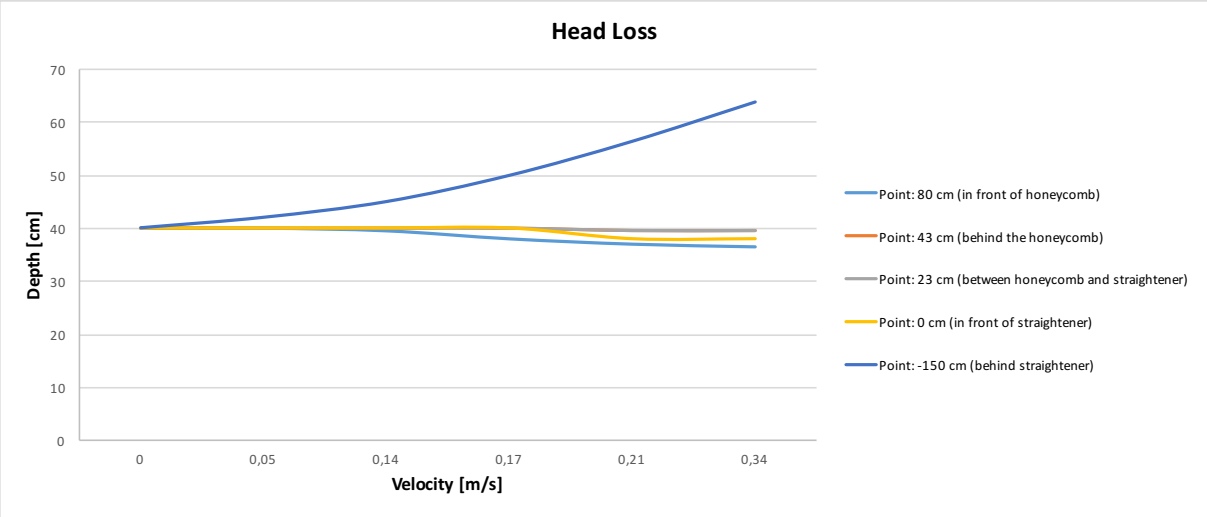

Figure 3.9: Head loss at different velocities

3.2.6 Error sources

All the measurements in the preliminary tests are preformed manually which makes them prone to human errors. The point gauge is exposed to technical errors in the instrumentation, for example from low battery levels. The measurements of free surface elevation are prone to wall effects in the flow, therefore these tests were performed in the middle of the flume to avoid errors. The simple velocity test was performed two times to ensure the same velocities were observed at both tests.

3.3 ADV (Acoustic Doppler Velocimetry) measurements

There exists several methods of mapping velocities in a fluid flow. In this thesis the method of Acoustic Doppler Velocimetry was chosen to find velocity profiles across the flume. The method was chosen because it was easy to use and post-processing of the results are not time

consuming or requiring a lot of data capacity. Previous experience in the use of ADV was also gained through the project thesis in Fall 2016. More advanced velocity measurement devices were also considered, such as Particle Image Velcimetry (PIV), but ADV was chosen to be the best option in this case. In the following sections the ADV experimental tests are presented.

3.3.1 Experimental set-up

Acoustic Doppler Velocimetry is based on the principle of the Doppler shift effect (Voulgaris et al., 1998). The ADV probe consists of four receivers and one transmitter as seen in the middle of Figure 3.10. The operation principle consists of transmitting short acoustic pulses through the transmitter. The acoustic energy is scattered back by small particles suspended as the pulses propagates through the water column. Using pulse-pair processing techniques the phase data ($d\phi/dt$) are converted from successive coherent acoustic returns into velocity estimates. Using the Doppler relation the phase data are converted into speed.

$$U = \frac{c(d\phi/dt)}{4\pi f} \tag{3.1}$$

where c is the speed of sound in water and f is the ADV's operating frequency. The phase data is derived in a more complex way due to the geometry of the probe and the turbulent nature of the flow. More details can be found in Voulgaris et al. (1998).

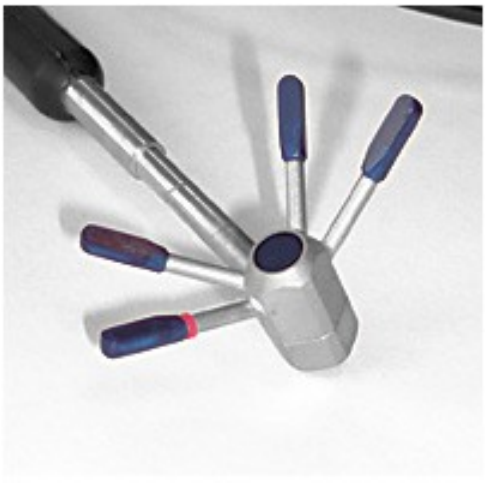

Figure 3.10: The Vectrino 2D-3D ADV Sidelooking Cable Probe(Nortek AS, 2016).

The Acoustic Doppler Velocimeter used is called Vectrino 3D water velocity sensor Lab Probe

from Nortek AS. The Vectrino is a high-resolution acoustic velocimeter. It can measure 3D water velocity in many applications from laboratory experiments to the field work in the ocean, and studies rapid fluctuations of velocity. The basis measurement technology is coherent Doppler processing, which is characterised by accurate data with no appreciable zero offset (Nortek AS, 2017). The specifications for the ADV can be observed from Figure 3.11, and more information about the technical specifications is presented in Appendix B.

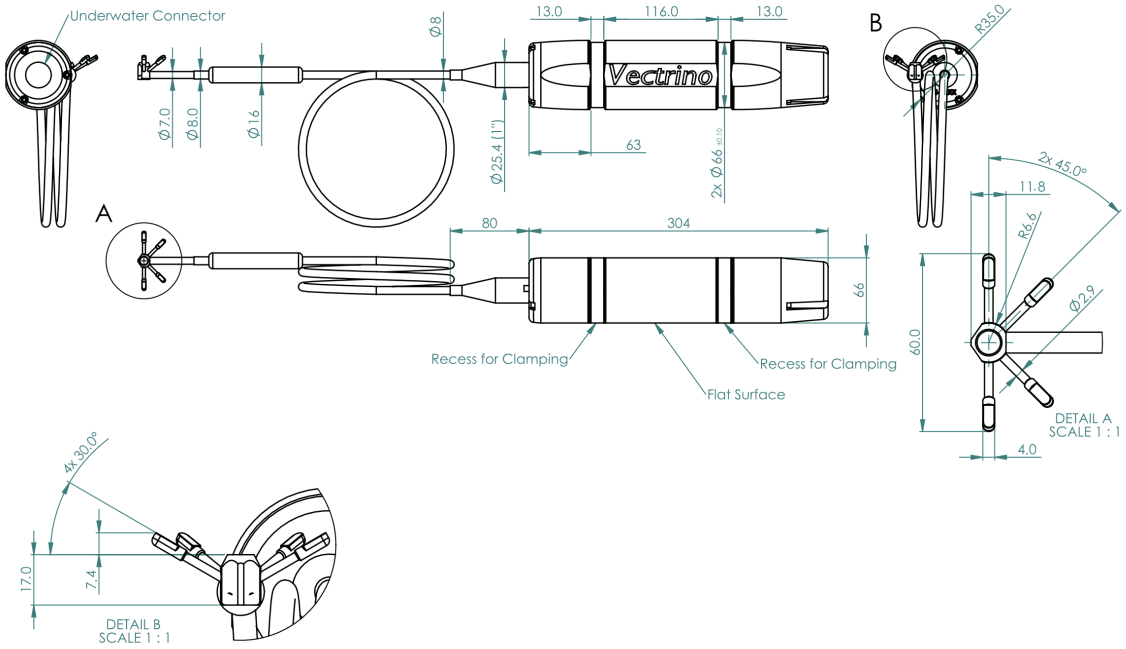

Figure 3.11: Sketch of the Vectrino 2D-3D ADV Sidelooking Cable Probe(Nortek AS, 2016).

For the ADV measurements a side-looking probe was used, because the flume bed gave the down-looking probe disturbing noise that influenced the quality of the measurements. The noise probably originated from metal plates underneath parts of the flume bed sections. A down-looking probe was used during the preliminary tests in the project thesis, which had results with many disturbances. For this reason as side-looking probe was preferred as the better option. The side-looking probe was always fronted by the glass walls of the flume, and was not prone to significant disturbances. Due to the application of two different probes the comparison of the previous data may not be valid. In order to obtain good results using ADV several requirements needs to be fulfilled. Seeding beams in the water needs to be at a decent

level in order to obtain acoustic signals of quality. For this reason seeding beams from the manufacturer of the ADV, Nortek, were added continuously throughout the testing. Right alignment of the probe to the flow, and no vibration in the set-up of the ADV is necessary to obtain decent results from the velocity testing. For this reason the ADV was mounted securely at the top of the flume tank.

The measuring firmware used was the Vectrino+ (Nortek AS, 2016). This is Nortek's own firmware configured with the ADV Vectrino. It has a maximum output rate of *25 Hz*, and allows collection rates up to *200 Hz*. The firmware makes it also possible to measure the distance to the bottom with sub millimetre accuracy at *10 Hz*. The firmware program makes it possible to visualise the collection of data while measuring to ensure the data collected is of quality. The data collection was observed throughout the testing to make sure the correlation level was higher than *90%* and the Signal-to-Noise-Ratio did not get lower than *5%*. The program also has settings to set time for the collection of data. The data in this test were sampled at *100 Hz*.

The vertical ADV measurements was taken at five points i x-direction, and three points for the cross-sectional measurements. The water depth was set to *40 cm*, and the flow velocity at *0.34 m/s*, the highest velocity. The data was collected for three minutes at each point measured in the flume. The velocity profiles were captured for the vertical direction (z-direction) and cross-sectional direction (y-direction). All the cross-sectional measurements were captured at *16 cm* depth because this is the most prominent position for the bulk velocity (Henry, 2016). The velocity profiles in the vertical direction consisted of seven measuring points vertically at five points in x-direction downward in the flume. These can be seen in Table 3.2. These points were chosen to avoid blind spots, that can affect the recordings of the ADV.

The measurements in vertical direction started *5 cm* above the bed due to limitations of the ADV close to the boundary of the flume bed. The cross-sectional velocity profiles consisted of five measuring points across the flume at three points in x-direction seen in Table 3.2. The measurements over the width of the flume had to be adjusted to a side-looking probe, so the results is adjusted to accustom this by removing the first measuring point in the result plots. The ADV captures the time average of the velocities and their fluctuations. This informations was also used to calculate the turbulent Reynolds stress at the three last points in the flume.

All the measurements had enough seeding beams to give an adequate dataset with a correlation of over 90%. The set-up for the velocity measurements are shown in Figure 3.12 and 3.13.

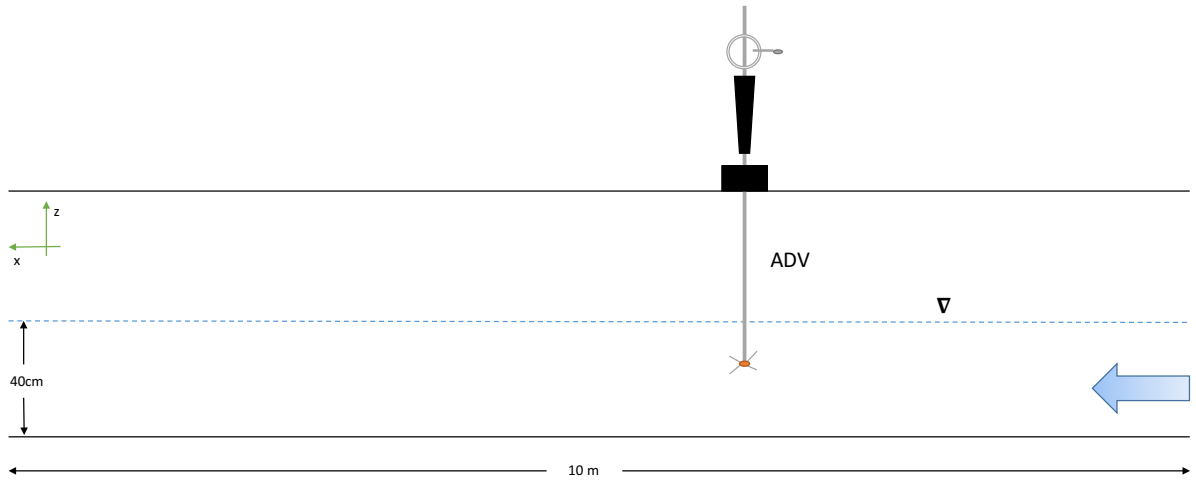

Figure 3.12: Experimental set-up for ADV measurements seen from the side of the flume.

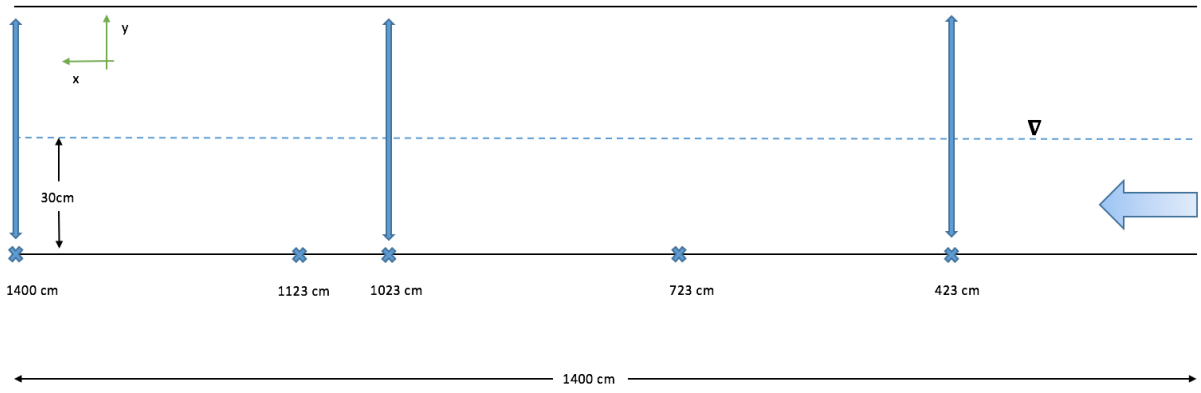

Figure 3.13: Measuring points in longitudinal (x-direction) and cross-sectional (y-direction) seen from above the flume.

Table 3.2: Measuring points for the velocity profiles

Vertical velocity profiles		Cross-sectional velocity profiles	
Point [cm] (x-direction)	**Depth [cm] (z-direction)**	**Point [cm] (x-direction)**	**Width [cm] (y-direction)**
423	5	**423**	10
723	10	**1023**	20
1023	15	**1400**	30
1123	20		40
1400	25		50
	30		
	35		

3.3.2 Data analysis and post-processing of data

When performing ADV testing it is necessary to post-process the raw data by filtering. This will improve the data-set and remove inaccuracies in the measurements. The software used for filtering was WinADV as recommended by Henry (2016), and previously tested in Fall 2016.

WinADV is a program for post-processing real time data files (*.adv files) recorded by the ADV. The program is valuable when used for field and laboratory studies since it offers powerful filtering and processing options. Guidelines from the article written by Wahl (2004) has been used throughout the filtering process and more extensive information about the filtering can be found there.

When filtering the raw data, the Signal-to-Noise-Ratio (SNR) and correlation parameter (COR) are of importance. In the article Wahl (2004) states that when investigating average flow velocities a SNR value of at least *5%* is recommended. The SNR value was set to *5%* for all the raw data post-processed. He recommends to remove all the correlation scores below *70%*, so this was implemented when filtering. He also states that values below a correlation of *70%* can still provide good data, but this is something to that is not investigated further here. A spike detection filter, called the phase-space thresholding method, is also used. The filtering removes single point spikes that are above or below the surrounding trend of data, multi-point spikes, and spikes that blend in with the surroundings (Goring and Nikora, 2002). The filtered data were plotted and visualised using Matlab. From the data set turbulent shear

stresses (Reynolds stresses) were also plottet in Matlab.

3.3.3 Results of velocity profile analysis

In the following sections the results from the ADV measurements to map the flow velocities are presented. The results are compared with velocity profiles obtained in the project thesis. These results will set the foundation for how the flow behaves in the flume, and gives an indication of how the flow will affect the plant motions in the final tests.

Vertical velocity profiles

The previous vertical velocity profiles from the project thesis are presented in Figure 3.14. The results had large velocity fluctuations, and a large amount of the data needed to be filtered out. The data filtered out were inaccuracies in the data recording from behaviour in the flow. This resulted in a coarse set of data that is probably not representative for the flow field in the flume. The results also showed a jet being observed in the flow, which possibly origins from the bad inlet condition.

During the Spring 2017 improvements were performed on the inlet of the flume. This resulted in a much straighter flow with small changes in the velocity. The results present velocity profiles that looks more similar to profiles expected from theory of open-channel flows. The data-sets were less filtered, which resulted in more even velocity plots as seen from Figure 3.15b. The flow is starting to develop at point *423 cm*, as seen in Figure 3.15a. The flow is fully developed at point *723 cm*, as seen in Figure 3.15b.

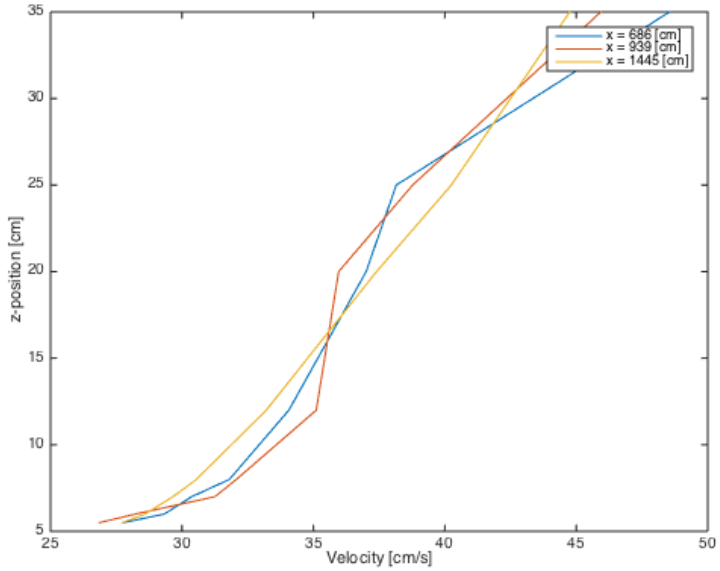

Figure 3.14: The mean velocity profiles in vertical direction from the ADV measurements performed in the project thesis in Fall 2016.

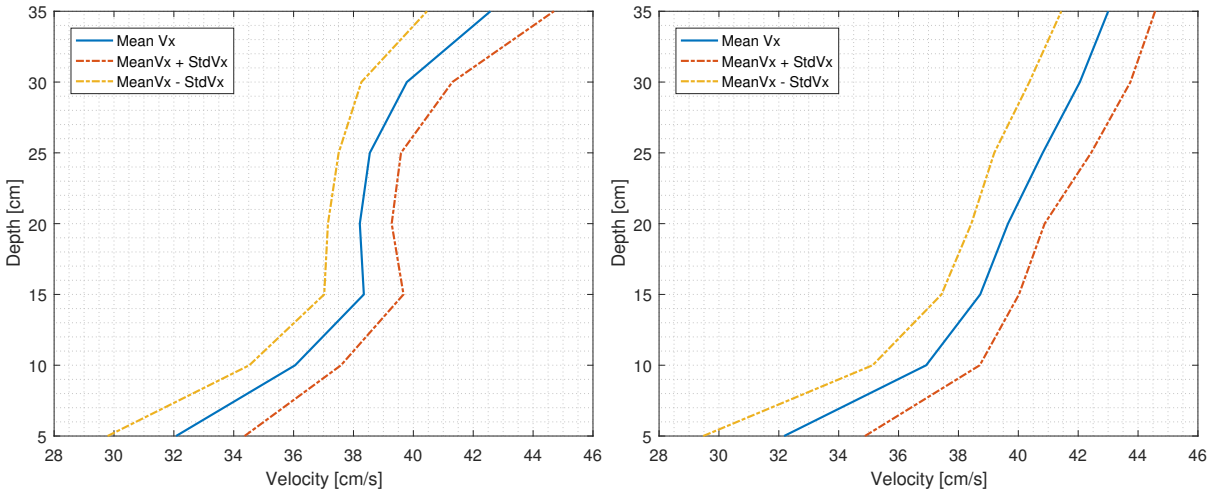

Figure 3.15: The mean velocity profiles in vertical direction at (a) 423 cm and (b) 723 cm.

In Figure 3.16a, 3.16b and 3.16c a change in the velocity profile occurs approximately at *30 cm* depth. This is can be an indication of second order effects occurring at the top of the flow water column. This inaccuracy occurs at the three point furthest down in the flume, and may be a result of the uneven flume bed creating eddies from viscous effects. The change arise in the ADV measurements around the same point where the flume bed had the most slope change, and for this reason also support that this can affect the flow. To confirm this observation further experimental testing are needed. An analysis of the turbulent Reynolds

stresses has been performed to investigate if it can give an indication of second order currents occurring at these points. More information on this phenomena is presented in the following Section 3.3.3 on turbulent Reynolds stresses.

Comparing the results obtained during the project thesis and the results given here for the ADV one can observe improvements in the flow. The new inlet design has made the fluid flow in the flume tank less prone to disturbances caused at the inlet. A jet is not occurring in the new flow regime, and the velocities observed gives a better understanding of the flow behaviour for the final tests.

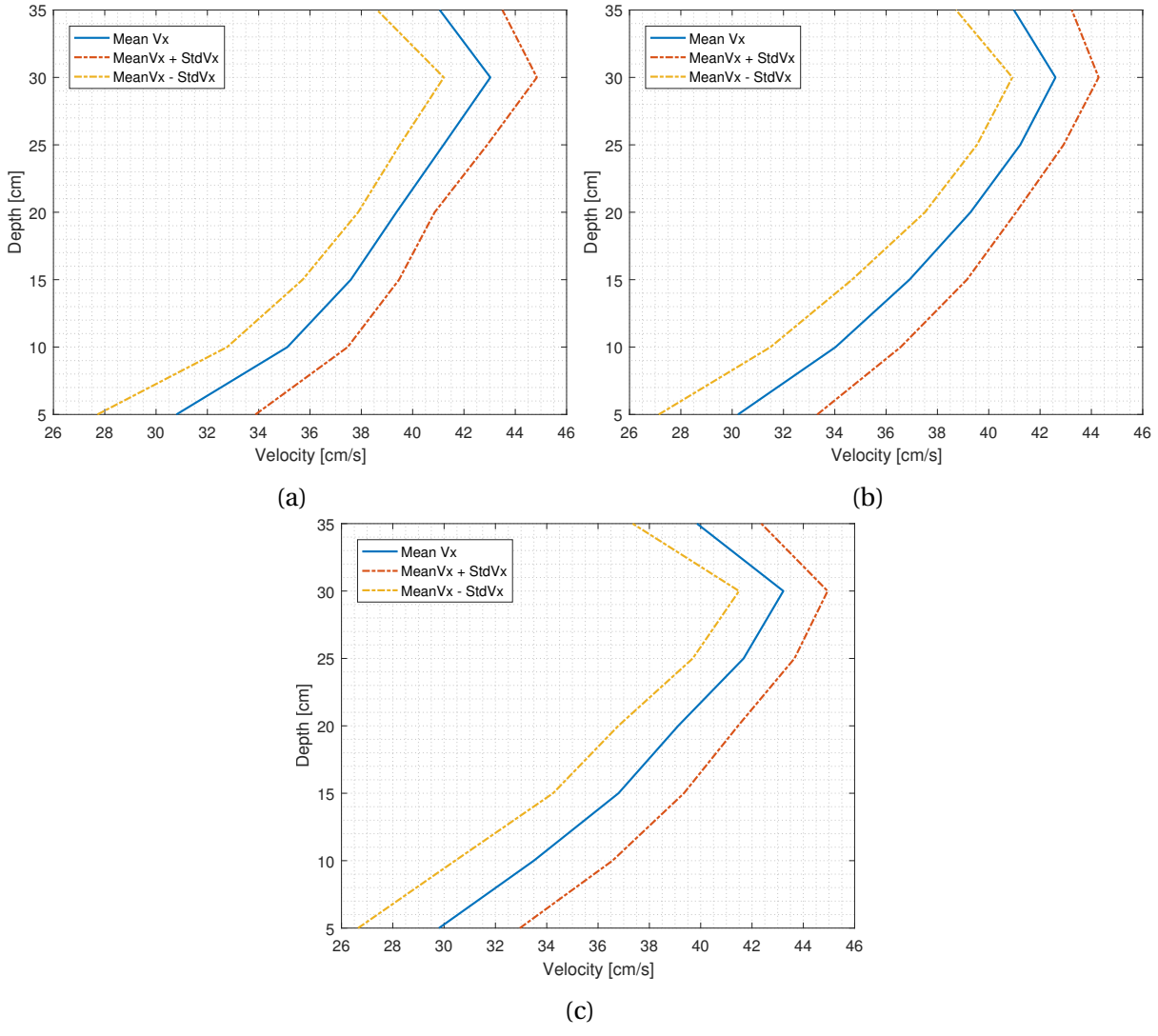

Figure 3.16: The mean velocity profiles in vertical direction at (a) 1023 cm, (b) 1123 cm and (c) 1400 cm.

Cross-sectional velocity profiles

The velocity profiles in cross-sectional direction, also showed an improvement compared to the the past tests. From the previous test one can clearly observe that the flow is not symmetric around the midline, and this indicates a disturbance in the flow, such as a jet, seen in Figure 3.17. The data are also too filtered to represent the fluid flow fully.

The results of the velocity profiles shows the profile being symmetric over the midline for the profile at point *423 cm* at the beginning of the flow, as seen in Figure 3.18a. For the two other points further down the flume a disturbance is seen such that the highest velocity is moved towards the right side of the flume, observed in Figure 3.18b and 3.18c. This effect can rise from the flume bed being uneven, and give disturbances that gets carried with the flow causing non-linear forces and second order current. The results of the cross-sectional velocity profiles supports similar observations as for the vertical profiles, but further testing is needed to confirm this indication. For the final tests these observations gives a foundation for the flow regime occurring across the flume, and helps to get an understanding of the flow behaviour.

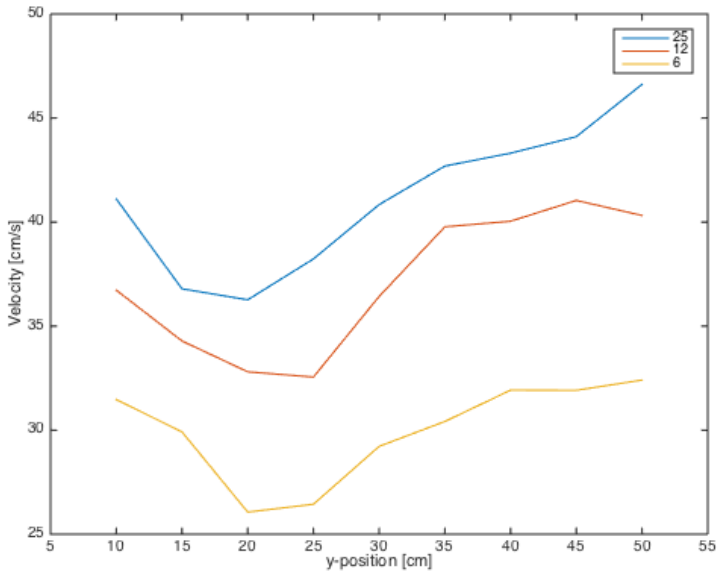

Figure 3.17: The mean velocity profile over the cross-section at $x = 939cm$ at three different depths

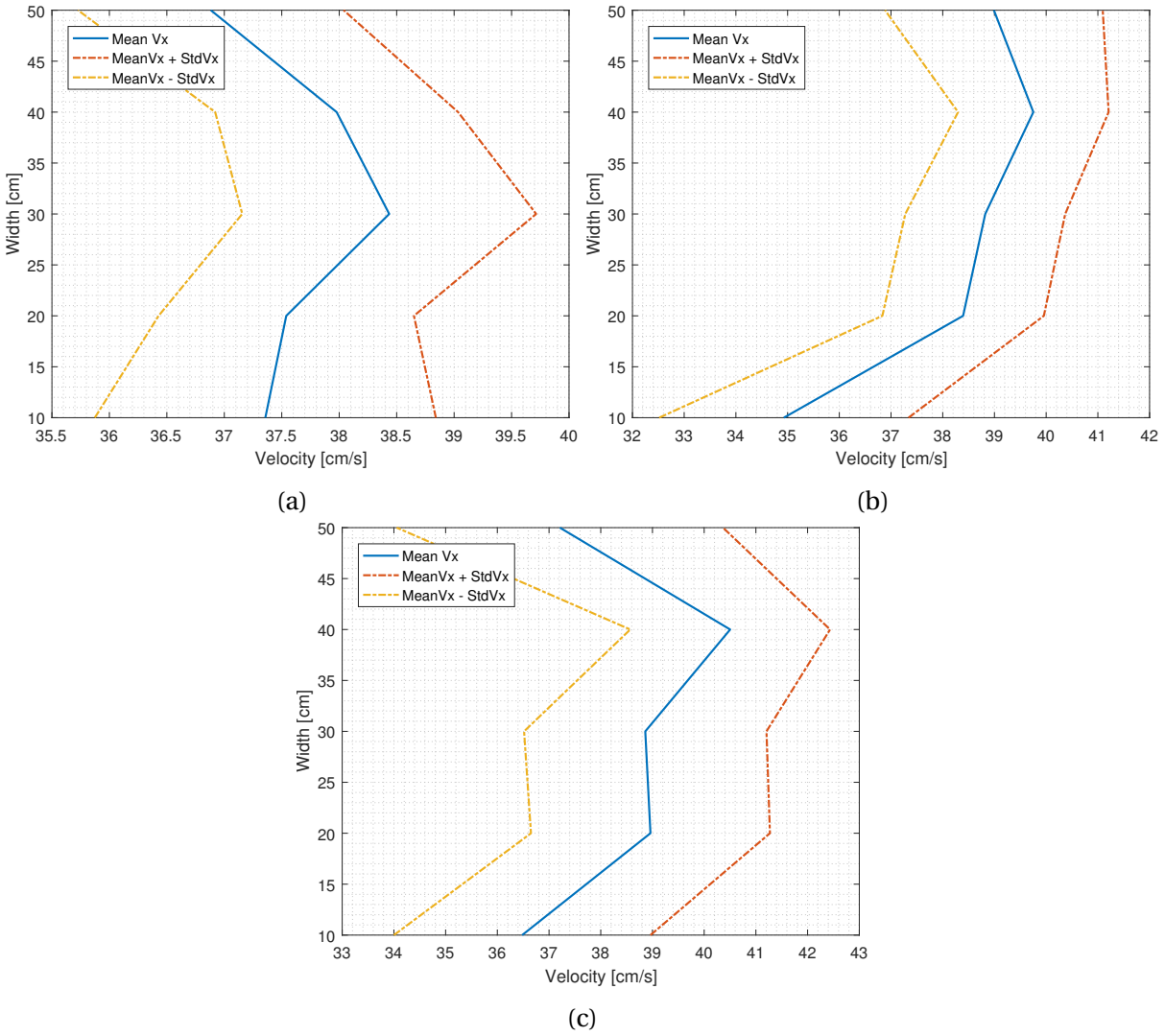

Figure 3.18: The mean velocity profiles in cross-sectional direction at (a) 423 cm, (b) 1023 cm and (c) 1400 cm.

Reynolds stresses

The results from the ADV velocity measurements gave an indication that the data sets were in decent condition, with little filtering needed. The changes at the top layer of the flow indicated in the three furthest points down the flume shows second order current occurring. Therefore, a Reynolds stress analysis was performed to investigate the turbulent shear stresses in the flow at these points. Figure 3.19 shows the turbulent shear stresses observed. The Reynolds stresses crosses zero at the x-axis, which gives an indication that second-order effects are present in the flume flow. If there existed no inaccuracies from shear in the flow the plot would have been similar to the one presented in Figure 2.12. The second-order effects can arise from disturbances mentioned before such as an uneven flume bed and other

inaccuracies, but this also needs further testing to be confirmed.

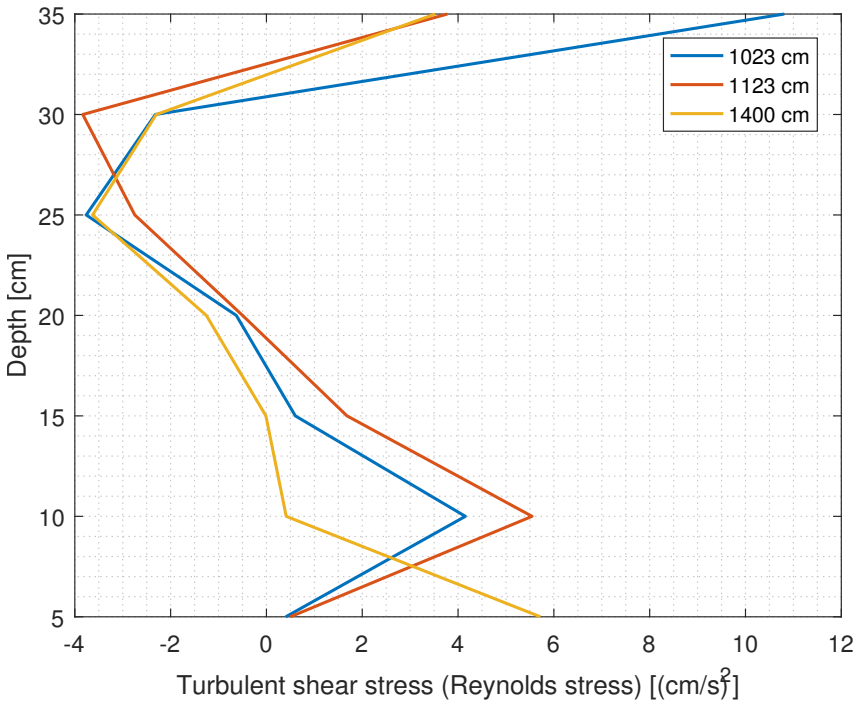

Figure 3.19: Turbulent shear stress

3.3.4 Error sources

The ADV is sensitive to different disturbances in flow. This can for example be uneven bed in the flume, different types of materials across the flume and not enough seedings in the flow. The alignment of the ADV is also of great importance. Misalignment can lead to errors, because the data needs to be align at the correct axis in the post-processing to get a good representation of the flow regime observed. The calibration of the ADV was performed beforehand, so there is no information about it and this can lead to errors. The ADV can also be sensitive to turbulent flow happening in the flow. Experimental testing with ADV in the flume can often give a portion of inaccurate data, so as mentioned filtering is needed. Filtering too many or too few data out can lead to errors in the result. As all manual testing the results are also prone to human errors. An error source of significance is possible fault in the instrumentation and data processing.

3.4 Surrogate modeling

Experimental testing of organic material is a complex process. When dealing with a living organism, such as a plant, there are challenges to overcome. In order to analyse the living plant in a correct way the condition needs to be as close to the natural living environment as possible. This is almost impossible to achieve in a lab environment, and the care of the plant tested would be too demanding due to husbandry (Frostick et al., 2014). Therefore, the solution to avoid this problem is to use a surrogate model. The surrogate model will mimic the behaviour of the plant to the extent that it gives enough useful insight to give a better understanding of how it behaves in different environments. This understanding will be sufficient in the early start of research on hydrodynamics of aquatic plants. The model can be used and tested in many situations, and is easy to make in many types of material. In this following section the method of how the surrogate model for the final tests were made will be presented.

3.4.1 Method

When making a surrogate plant model of the kelp *Laminaria Digitata* there are important aspects to consider. The surrogate model needs to mimic the complex plant behaviour in a correct way. Therefore, the material of the model is of great importance. The surrogate plant model is only *40 cm*, in comparison to the real plant, which is up to 2 meter, with a blade length of *22 cm* and width of *9 cm*. The diameter of the stem varies from *1.2 cm* at the bottom to *0.8* close to where the blade starts. To mimic the plant behaviour different materials with a variety of hardness were chosen ranging from Shore A Hardness of 20A to 90A. The variety of hardness where chosen on the basis that when the plant model is scaled down the material should be stiffer, and may mimic the natural plant movements better. A variety of different materials were tested and the materials is listed in Table 3.3. All the materials were chosen from the brand Smooth-on, except the TFC 3014 which is from Trollfactory. Only three surrogate models in different materials were chosen for the final model tests.

Table 3.3: Technical overview of the different materials used to cast the surrogate model.

Technical Overview	TFC 3014 abformsilikon	Smooth-Sil 935	PMC-746	PMC-780 Dry	PMC-790
Mix Ratio	1A:1B	100A:10B	2A:1B	2A:1B	2A:1B
Mixed Viscosity (cps)	4 000	30 000	1 200	2 000	3 000
Specific Gravity (g/cc)	1.1	1.18	1.03	1.02	1.07
Specific Volume (cu. in. /lb.)		23.5	26.9	27.2	25.9
Pot Life	6-8 min	45 min	15 min	25 min	20 min
Cure Time	40 min	24 hrs.	16 hrs.	48 hrs.	48 hrs.
Color	Mint Green	Blue	Amber	Light Amber	Clear Amber
Shore A Hardness	20A	35A	60A	80A	90A
Tensile Strength (psi)		650	700	900	>2 000
100% Modulus (psi)		170	220	400	640
Elongation at Break	380%	300%	650%	750%	550%

A mould previously made by Henry (2016) was used to make the surrogate model. The mould is made in plexiglas, and forms a simplified model of the kelp *Laminaria Digitata* as seen in Figure 3.20a. The mould was *46 cm* heigh and *19.2 cm* broad. The mechanism when making the model is to use a vacuum chamber to suck the liquid material inside the mould, as seen in Figure 3.20b. The process is carried out by using a vacuum pump creating vacuum in a chamber also made of plexiglas. The silicone material needs to be vacuumed for three minutes before it gets sucked inside the mould. The materials had different curing time ranging from 20 minutes to 48 hours. Only three models were successful in the end to be used in the final testing, because this way of making the surrogate models is not ideal as it is prone to faults. This will be discussed in the following procedure of making the surrogate models.

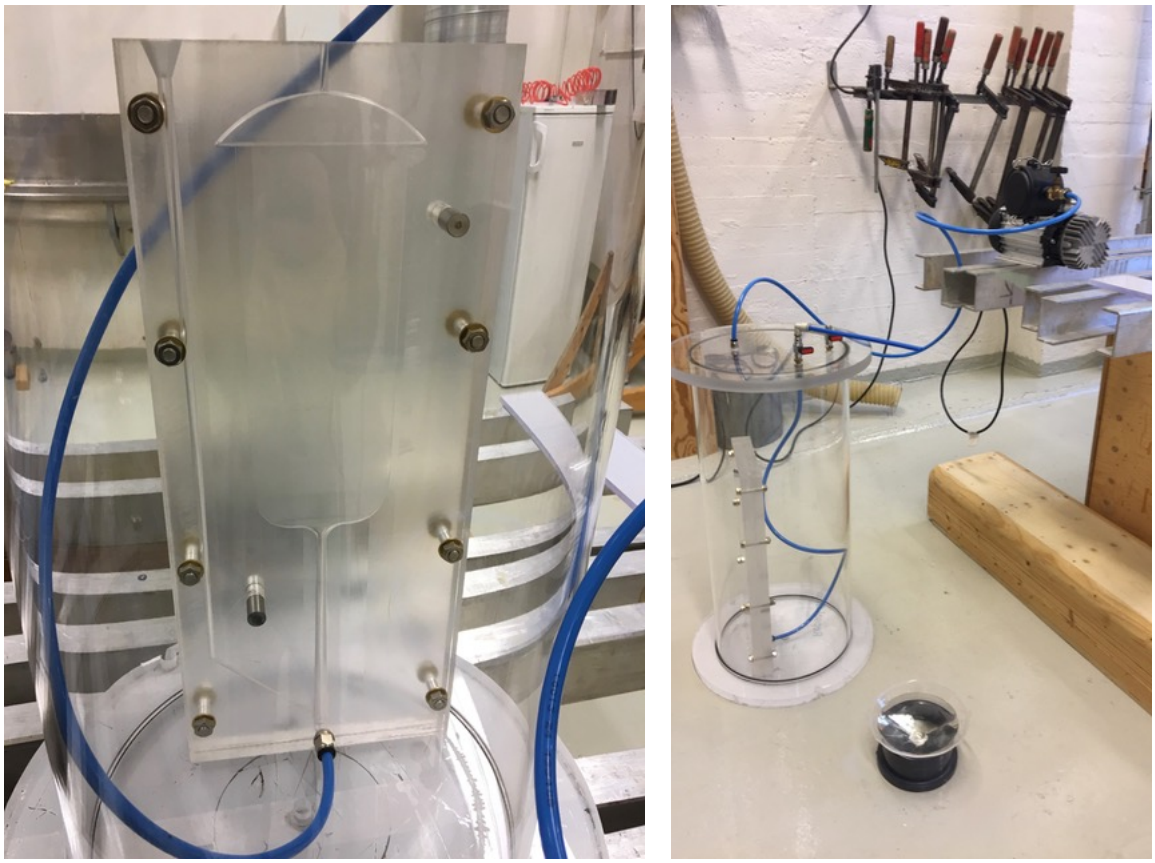

(a) (b)

Figure 3.20: The mould and set-up of the surrogate modeling (a) the mould of the simplified surrogate model of the kelp *Laminaria Digitata*, and (b) the set-up when making surrogate models with the vacuum chamber surrounding the mould.

The procedure of making the surrogate model is as follows. Firstly, the material needs to be mixed according to the instructions given by the provider. All the materials used are supposed to be mixed at a temperature of 23 degrees celsius. The mixed material is then vacuumed in a chamber for approximately three minutes in order to get trapped air bubbles out. The time will depend on how viscous the liquid of the material is. After vacuuming, the liquid is sucked into the mould using a vacuum pump. When doing this the mould is put into the vacuum chamber. This procedure is prone to difficulties. Some of the materials used have varying viscosity, which make the ones with high viscosity difficult to suck inside the mould. To omit this difficulty different techniques were tested included putting the mould upside down to make gravity help the suction. The mould is also prone to air leakage. This resulted in several unsuccessful attempts making the models as shown in Figure 3.21.

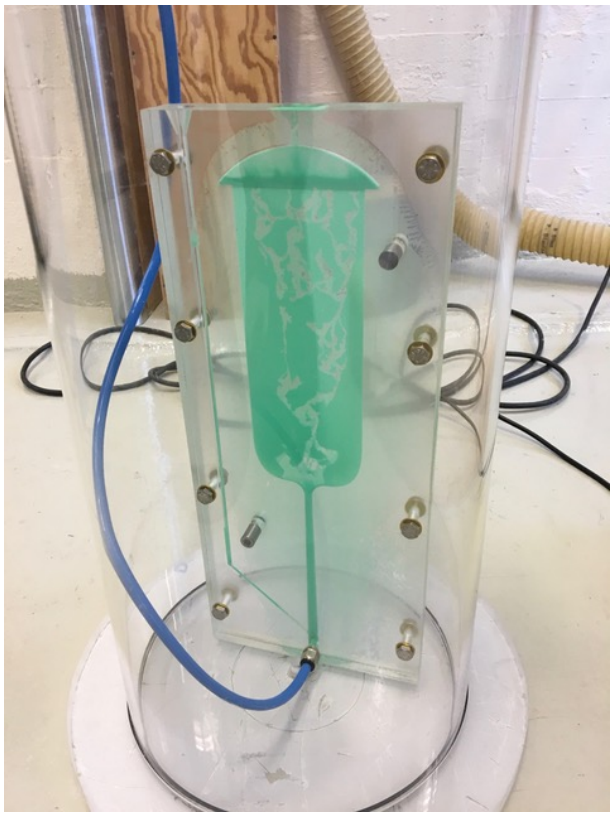

Figure 3.21: A failed attempt on making a surrogate model i hardness 20A.

After several attempts of different materials, only three models were successful. A model with Shore 20A, 60A and 90A. Both the model with 20A and 90A have some holes in the blade, so the significance of this flaw remains unknown, as there are no models to compare the results with. The model with hardness of 60A is in the best condition with no holes or other fractures. The different surrogate models are seen in Figure 3.22a, 3.22b and 3.22c. The models who came out unsuccessful had either air bubbles in the stem or holes in the blade, which is not desirable for testing.

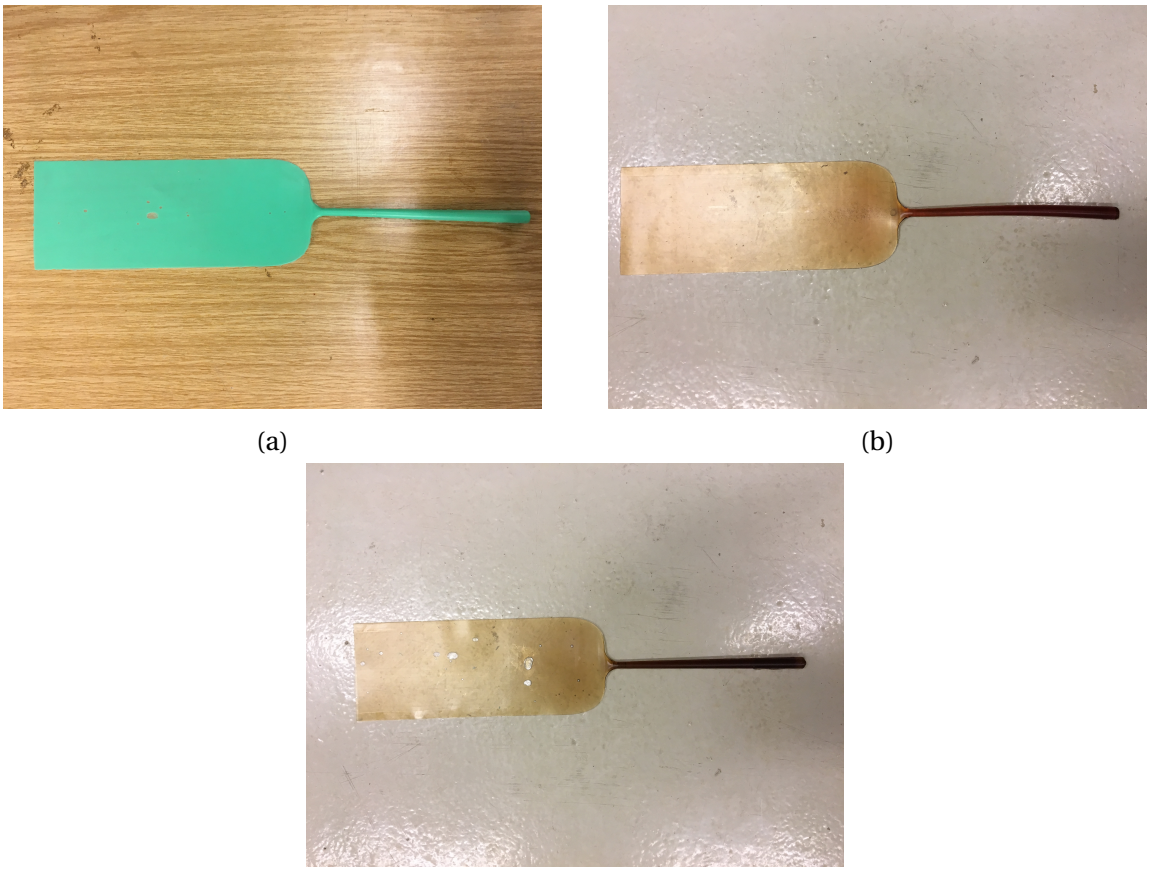

(a) (b)

(c)

Figure 3.22: The three surrogate models in different material used in the model tests (a) Shore hardness 20A, (b) Shore hardness 60A, and (c) Shore hardness 90A.

Before testing a mount was installed at the bottom of each stem to fasten in the flume. In the surrogates with 20A and 90A it was difficult to get the mount to stick inside the stem, therefore a safety plastic zip tie was put at the bottom of the stem on these models. The mount is seen in Figure 3.23.

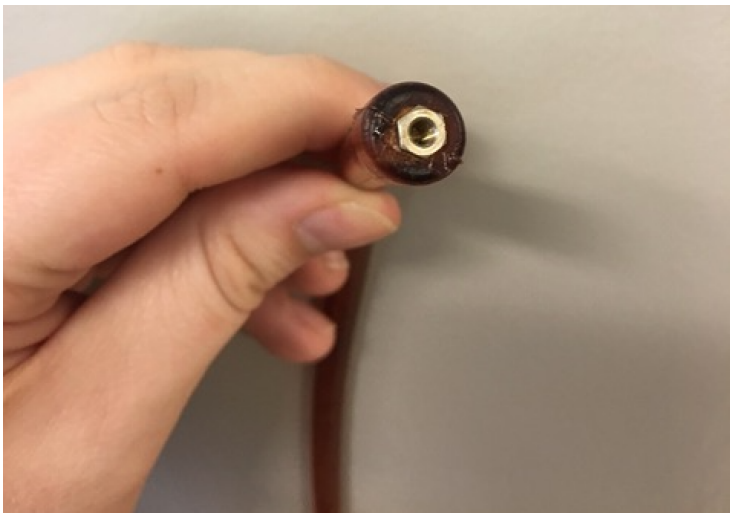

Figure 3.23: The skrew mount at the bottom of the surrogate model.

3.4.2 Error Sources

When creating surrogate models of different material the goal is to mimic the behaviour of the actual plant in the best way. Inaccuracies in the model, such as wholes and dents, can affect this behaviour. Scaling issues are also a possible error source. The manual modelling is prone to humane errors, due to the difficult procedure of making the models.

Chapter 4

Model tests

In this Chapter the final experimental tests are presented, the plant-flow interaction observations and the drag test. The test were performed in the flume tank at the flow conditions investigated in the preliminary testing. The results and discussions are presented at the end of the Chapter.

4.1 Experimental set-up

The model tests were performed with three different surrogates. The tests were performed over two days in May 2017. Plant-flow interaction tests at different velocities were performed and a drag force test on the surrogate 60A. The surrogate 60A was drag force tested because it was the only model with no fractures in the structure. The models were tested and filmed for five minutes at each flow condition. The surrogates were mounted at *x=1163 cm* down the flume. The drag force measurement device was a F/T sensor. The sensor model is called *Nano17 IP65/IP68* as shown in Figure 4.1. The sensor was placed at point *[*1163 cm] and mounted by a screw to the model plant stem. The force sensor is extremely sensitive and if exposed to invasive handling it can easily brake. Therefore, precautions must be taken when handling the force sensor. The sensor captures both fluid forces, in this case drag, and torque of the structure exposed to flow. The finest calibration of the sensor was performed before the final tests. More information on the technical specifications of the sensor are given in Appendix..

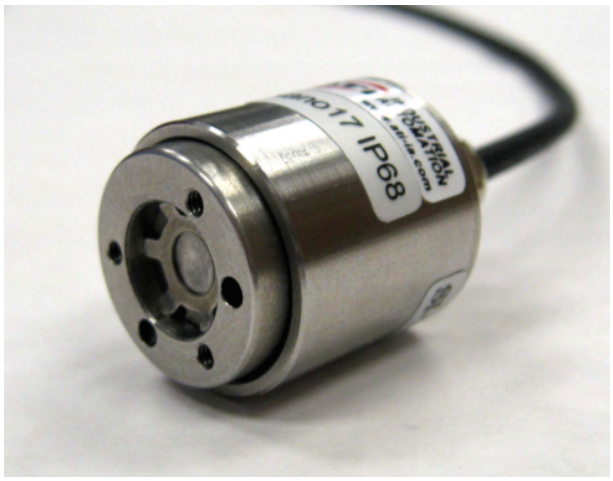

Figure 4.1: The drag force sensor Nano17 IP65/IP68 (ATI-Industrial-Automation, 2017).

For the visualisation of the plant-flow interactions, three cameras were used. One set up at the side of the plant, on above and one captured the motions from behind the plant reflected by a mirror downstream in the flume. The mirror was angled such that the camera was positioned perpendicular to the mirror to avoid image distortion. The camera above the plant model was a waterproof GoPro camera with a wide angled lens. This can give distortion of the real image recorded, but the recordings were only used in observing motions, so a little distortion is valid in this case. Only surrogate 20A was tested with recorded video from three cameras, this was because this was the only plant able to be filmed due to its vibrant mint colour. The set-up in the flume is illustrated in Figure 4.2. The camera set-up is presented in Figure 4.3a, 4.3b and 4.3c.

The colour of the plant models of hardness 60A and 90A made it difficult to capture the motions from behind the plant, so only two cameras were used to capture the motions of these models. A LED light was set up to make the view of the plants better, but due to scratches the LED light was only beneficial to use for the surrogate plant model 90A. The scratches at the flume wall also made it difficult to observe the motions when acquiring the frequencies of the plant stem.

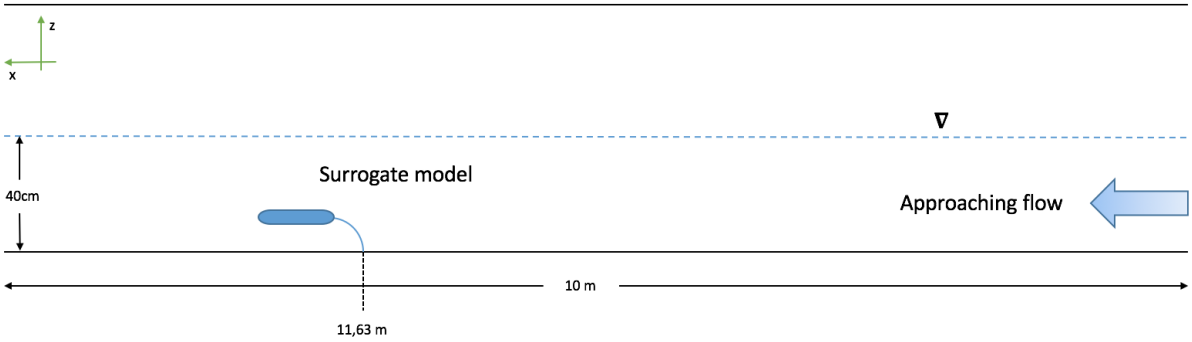

Figure 4.2: Experimental set-up of the model tests with three different plant models.

(a)

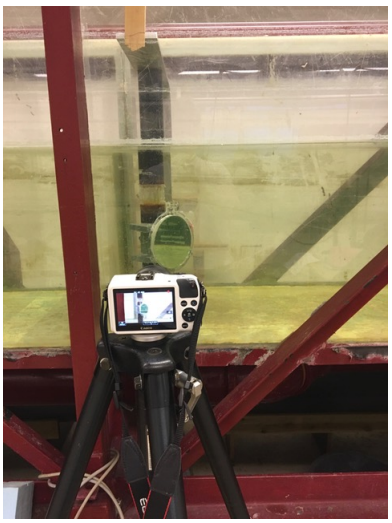

(b)

(c)

Figure 4.3: Set up for the video cameras capturing plant motions (a) at the side with the LED light, (b) behind with the mirror, and (c) above.

4.2 Data analysis and processing

The videos captured at the different runs were studied, and the plant frequencies were captured by viewing the motions directly from the video. The drag forces were captured using a F/T sensor, and the data are post-processed in Matlab.

4.3 Error sources

When performing model tests of flow behaviour in a laboratory flume there are potential error sources to look out for. In this case many of the error sources are connected to the laboratory flume. In short, the flume is old and have flaws that can affect the results. An example is the varying slope of the flume floor. This can give vortices in the fluid flow, that can lead to second-order forces that will give uncertainties in the results. The videos can give distortions that do not exactly represent the real world in regards to motions captured on film. The set-up of the plant model and construction of the surrogates can give potential errors in regards to natural representation of plant behaviour.

The drag test have also error sources to be aware of. The alignment of the plant mounted on the drag sensor is complicated to get completely correct. This can give errors in the results of the drag forces. The error is estimated to be approximately around 10 degrees of misalignment form the plant to the force sensor. The measurements are also a prone to human errors in the set-up and performance of the experimental testing.

Chapter 5

Experimental results and discussions

In this chapter the experimental results from the model tests are presented. The results are divided into two parts; the plant-flow interaction test and drag force test. The results are presented with a general discussions regarding all the finding, and how they compare to previous experimental studies and theory in Section 5.1.3.

5.1 Results of laboratory experiments

The results of the plant-flow interactions and drag forces represents the behaviour of the surrogate models influenced by the flow regimes tested. The observations and experimental testing performed in this thesis is not to be seen as a exact representation of the natural plant behaviour in real life, but rather an indication of how these types of plant would behave when exposed to different velocities ranging from *0.05 m/s* to *0.35 m/s*. Sequences of picture of each surrogate model are presented in the result at *0.34 m/s*, as this displays the largest motions. The rest of the picture sequences are presented in Appendix A.

5.1.1 Plant-flow interaction

Surrogate 20A

The surrogate model 20A was the most flexible model. This was also observed from the model test by it being the model with the most flexible movements when exposed to the flow. This was the only model that lied almost streamlined to the flow at calm water. When exposed to the smallest velocity, *0.05 m/s*, the plant model immediately streamlined in the flow. With increasing velocities the plant stem started to oscillate, and the blade motions seemed to affect the movements of the stem.

The reason for this behaviour can be explained by the undulating of the plant blade. This is when the blade contracts like an accordion in the flow. This movement affects the stem by the forces being transferred over the blade resulting in a oscillating motion of the stem. This plant model also had a tendency to move from side to side in the tank (y-direction). These motions may be caused by a second-order current creating vortices making the plant move sideways and twisting, as observed in the third picture frame in Figure 5.1. The sideways behaviour can indicate that the previous observations of vortices being created further down the flume may be correct, but further testing is needed to confirm this behaviour. Figure 5.1 presents the behaviour observed at the highest velocity. The model was the only one filmed by three cameras, but due to the flume tank wall having many scratches it was difficult to record video with good quality. For this reason one was not able to use the motions to find parameters like drag forces theoretically from observation. The two video camera angles is presented in Figure 5.2a and 5.2b. The picture series for the four other velocities are presented in Appendix A.

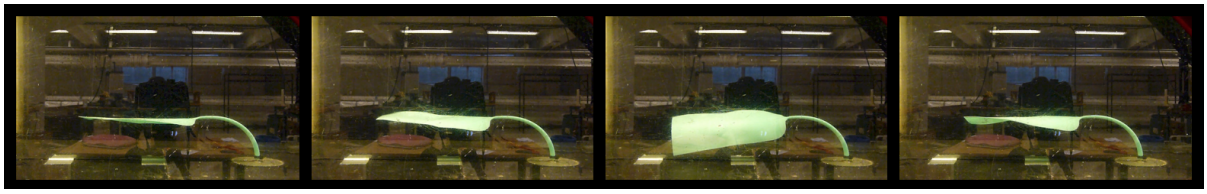

Figure 5.1: Motions of the 20A surrogate model in *0.34 m/s* flow.

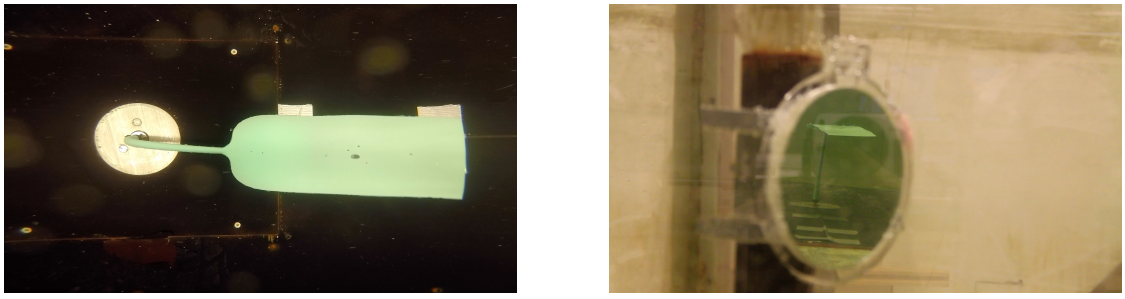

(a) (b)

Figure 5.2: Two of the video camera angles at the surrogate 20A (a) overhead camera view, (b) the back-view through the set-up mirror.

Surrogate 60A

The surrogate model 60A was made in the second hardest material, and was standing straighter in calm water. This surrogate was the only one made completely without any holes and

fractures, which made it ideal for the drag testing. These results are presented in Section 5.1.2. When exposed to the smallest flow rate the blade streamlined, but the stem was almost standing straight in the flow. It had only a small angle. As the flow velocity increased the plant model streamlined further, until the plant was fully streamlined as observed from Figure 5.3. This plant model was only recorded with two cameras, as the recording was rather weak as seen from Figure 5.3. Sideways movements were minimal, and can barely be noticed through the camera above the plant. The blade did also undulate at the higher velocities, *0.21-0.34 m/s*. The undulating motion seemed to dominate the plant stem oscillations for the higher velocities. Picture sequences for the rest of the velocities are found in Appendix A.

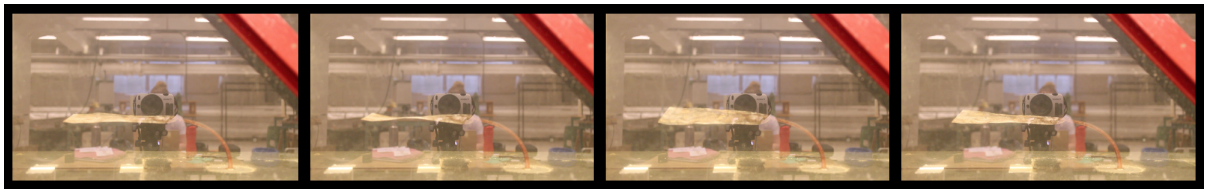

Figure 5.3: Motions of the 60A surrogate model in *0.34 m/s* flow.

Surrogate 90A

The kelp surrogate 90A was the model with the stiffest material, and was standing almost completely straight in the flow. The model is *40 cm*, so the upper part of the plant blade was touching the free surface. As the velocity increased the plant streamlined, but the blade did only fully streamline at the highest velocity *0.34 m/s* as seen from Figure 5.4. The stem did only streamline with a small angle at the highest velocity due to the materials stiffness. To obtain decent recordings of the plant movements a LED light was used to capture the movements as the plant model was in an amber colour difficult to capture on video as seen i Figure 5.4. The material of the plant model is really stiff the blade did not undulate, but had smaller movements for the higher velocities. The stem had smaller oscillating motions, and seemed dependent on the motions of the blade. The rest of the picture sequences of the other velocities is presented in Appendix A.

Figure 5.4: Motions of the 90A surrogate model in *0.34 m/s* flow.

Frequency analysis

All the plant models oscillated in the flow, which made it possible to capture the frequency of the surrogates in vertical direction. The frequencies were captured through observing the video recordings of the top part of the stem right after the blade. This makes it subjected to human error. The three models behaved differently when exposed to the flow. The surrogate 20A had the largest movements in the flow, and was the easiest to capture the frequency of. As the two other models were stiffer the movements were subjected to more oscillations. Non of the stems oscillated with an amplitude more than the stem diameter.

For the two smallest velocities the movements of the surrogate 90A were not noticeable and for this reason are set to zero at these flow rates as seen in Figure 5.5. The models 20A and 60A had similar frequency behaviour in the smallest flow velocities. As the velocity increased the frequencies started to approach a similar value. This behaviour is unusual as the materials are quite different. The frequencies at higher velocity could be a result of lock-in on the models in the flow. Therefore, a comparison with the shedding frequency was performed presented in Figure 5.6. If lock-in was occurring the shedding frequencies would lock-in at similar frequencies as the ones occurring for the plant models at higher velocities. This is not the case here, and indicates that there is something else dominating the frequency. An explanation for this observation could be that the plant model stem is dependent of the blade movements for higher flow rates. In this case it is not the vortex-induced vibrations that are causing the movements of the stem, but rather the blade itself when it is undulating in the flow. More analysis is needed to confirm that this observation represents what is occurring in reality.

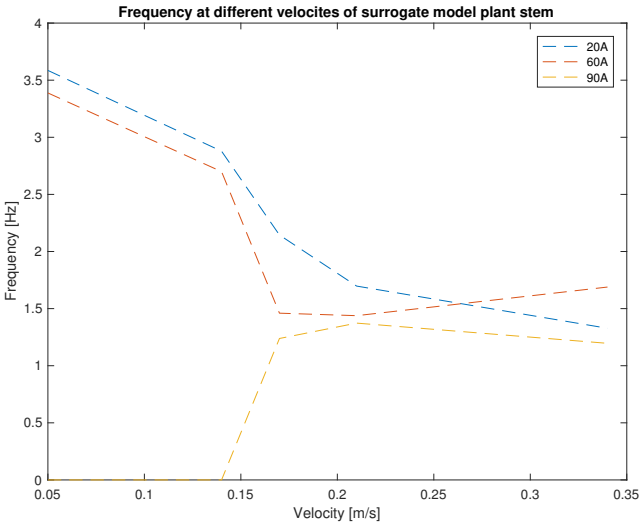

Figure 5.5: Mean frequency of the top stem of the surrogate models

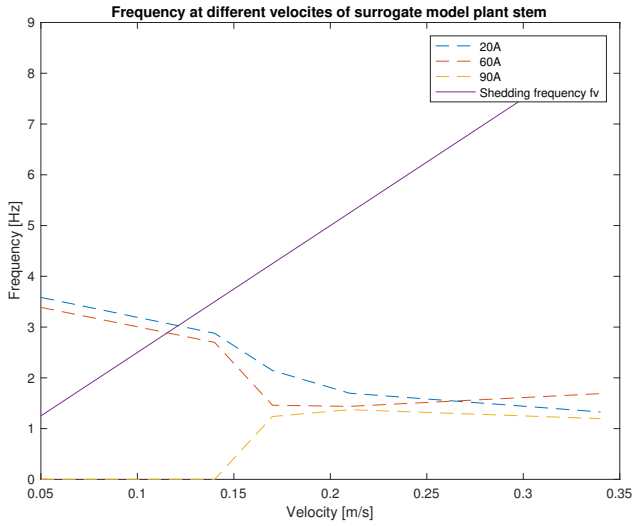

Figure 5.6: Mean frequency of the top stem of the surrogate models with the shedding frequency.

5.1.2 Drag forces

Drag forces were measured on the model surrogate 60A. The drag forces of the surrogate model are in a similar range with the drag forces observed in (Albayrak et al., 2014), but a bit higher. The plant shoot tested in that study was shaped like a tall sea grass. This difference can explain why more drag is experienced in the measurements in this thesis. The blade will contribute to giving the plant model a higher drag force. The drag increases with the velocity

as to be expected. In theory the drag force increases with velocity squared. In the model test of the drag force this correlation is not observed, and is the same observation as in (Albayrak et al., 2014). An explanation for this observation is that the rule only hold for high Reynolds numbers. In this case the velocities are low, and the Reynolds number is not significantly high for this relation to hold.

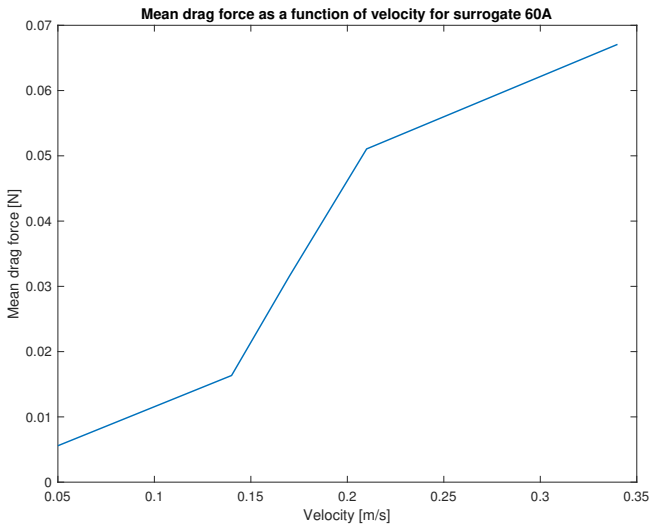

Figure 5.7: The mean drag forces on the surrogate 60A exposed to flow with velocities from *0.05 - 0.34 m/s*.

5.1.3 General discussion

The results reported in this master thesis brings discussions on both plant behaviour affected by the flow, and the flow regime around it. In this section a discussion about the findings are presented.

There exists no directly similar experimental research regarding this type of plant kelp testing in fluid flow, but findings from similar experiments may be taken into account. Henry (2016) has performed an experimental study on how this type of surrogate plant model affects the flow around it. His study also found that the flexible structures streamlined when exposed to flow depending on the material properties. This is the same observations as found in the plant-flow interaction tests of the surrogate plant models. This the streamlining naturally occurring when a flexible structure is exposed to fluid flow to minimise the forces. The difference in material composition is the property defining how the flexible structure will streamline.

In natural fluid flow in the habitat of similar plants the flow will have vortices, and turbulence affecting the behaviour. The results showed the plant models in the flume reacting to these types of inaccuracies indicating that the movements came from non-linearities in the flow around the structure. A flexible blade will be affected by changes in the flow, and especially for the highly flexible model surrogate 20A. Wall effects in the flume, uneven bed and other disturbances may cause changes in the flow affecting the model behaviour.

Another interesting observation is the oscillations of the top stem that may be caused by the movements of the blade in the flow. As previously assumed, VIV and lock-in were assumed to be the dominating contributors to the oscillating motions as indicated in previous flow experiments on circular cylinders (Bearman, 2011). The result of the frequency of the plant with the shedding frequency may indicate that in this case the plant stem oscillations of the flexible structure depend on the blade movements. This is an interesting observation that needs more investigations to find if the blade is actually dominating the stem oscillations. The drag forces is within the range expected for this type of plant model when compared to the previous research of Albayrak et al. (2014). The drag is higher because the blade of this plant model is bigger than a tall sea grass. More detailed research on drag is needed to map how the drag behaves on surrogate with different material.

In these complex experimental plant testing it would be beneficial to have more information on the non-linearities occurring in the flow, as observations show they are dominating some of the motions. By using more advanced theory one would probably be able to explain the intricate behaviour of the plant models improving the knowledge on plant-flow interactions. Comparison testing with real kelp would be necessary to confirm if experimental testing on simplified plant model surrogate represents the nature of the plant. An improvement of the experimental testing facility would also benefit the quality of the results with a higher accuracy in the testing equipment.

Chapter 6

Conclusion and recommendation for further work

6.1 Summary

Through the course of this master thesis many aspect of plant-flow interactions have been investigated. A thorough background have been presented looking into the advantages of this resource. A literature review have been given in order to investigate previous research on plant interaction in flow. The theory behind these flow processes were also presented to make a foundation for the laboratory experiments. Surrogate models were made in different material to represent a simplified version of the kelp *Laminaria Digitata*. A preliminary flow mapping have been carried out, and was performed to investigate flow regimes of the velocities used in the final model tests. This set a foundation for the final testing. The final plant-flow interaction model tests were performed investigating both surrogate model behaviour affected by the flow, and drag forces on one surrogate model.

6.2 Conclusion

In the present work experimental studies of plant-flow interactions, plant model behaviour and drag forces have been carried out. The main conclusions are that for the three different surrogate plant models the plant posture changed with increasing velocity, and all the models streamlined for high velocities. This agrees with previous studies. Second-order effects appearing in the flow were also affecting the behaviour of the plant models, especially the most flexible surrogate 20A. The most interesting observation, is that the plant-flow interactions are probably dominated by forces arising at the blade scale when undulating, creating

oscillation at the stem. The results of the frequencies of the oscillating plant stems indicated no correlation with vortex shedding, when comparing to the vortex shedding frequency. This is a different observation from the previous assumptions where the plant stem oscillations are dependent on vortex-induced vibrations and lock-in effects caused by the flow. In this case the flexible structure of the plant model behaves differently than a circular cylinder in the flow, and detailed research is needed on to confirm if the stem gets affected by the blade motions. The drag forces were in the range expected, but not following theoretical drag velocity laws. Investigations on plan-flow interactions are complex, and from experience with these experimental tests, it needs a higher quality facility and equipment. Another contribution that would benefit research in this field is the ability to compare with real plant motions affected by the same flow regime. Consequently, further detailed research is necessary to confirm that the findings in this thesis can actually represent the natural behaviour of the real plant.

6.3 Further work

This section presents recommendations for further work on the basis of experience and knowledge gained from this experimental research:

Find improved method for making surrogate models

One of the main tasks in this master thesis was to make surrogate models for model testing. New materials were used and it caused problems with the mould. Especially, harder materials were a problem creating air bubbles that is not beneficial when mimicking the structure of a living plant. Therefore, a new improved way of making models would have been beneficial in order to obtain good surrogate models in a range of different materials.

Do extensive testing

Time is limited when working with a master thesis, and in experimental work one would always like more testing to increase the knowledge. The topic of hydrodynamics of aquatic vegetation is a fairly new one, and needs extensive testing in order to confirm the observa-

tions. For this reason further testing over a longer period of time is suggested. This will give an even better understanding of if the actual observations are the same ones happening over time.

Testing with different flow conditions

In this thesis the model tests were performed with a steady current with a range of velocities. A suggestion would be to test with a range of wave conditions, waves and current, and change the bed from smooth to different roughnesses.

Change the morphology

A change in morphology in the plant surrogates will give information on how this change affects the movement of the plant. The real plant *Laminaria Digitata* has many narrow blades, and a morphological change will mimic this in a better way. The blades could also be changed to mimic different types of kelps, and different materials could be tested for the blade and the stem.

Improve testing facility

The test facility used was a old one lacking of new technology and updated instrumentation. For example, the flume had no way of changing the velocity without doing extensive test to find the velocity at the given condition. It also did not have a self-cleaning system for removing sediments or other fragments in the flow. A higher quality facility would give more control over parameters controlling the flow, giving improved results.

References

A.H. Techet (2004). 13.42 lecture: Vortex induced vibrations. https://web.mit.edu/13.42/VIV_2004.ppt/. [Online; accessed May 20, 2017].

Albayrak, I., Nikora, V., Miler, O., and O'Hare, M. (2014). Flow–plant interactions at leaf, stem and shoot scales: drag, turbulence, and biomechanics. *Research Across Boundaries*, 76(2):269–294.

Alben, S., Shelley, M., and Zhang, J. (2004). How flexibility induces streamlining in a two-dimensional flow. *Physics of Fluids*, 16(5):1694–1713.

ATI-Industrial-Automation (2017). Strouhals vs. reynolds. http://www.ati-ia.com/products/ft/ft_models.aspx?id=Nano17+IP65%2FIP68. [Online; accessed June 1, 2017].

Bearman, P. W. (2011). Circular cylinder wakes and vortex-induced vibrations. *Journal of Fluids and Structures*, 27(5):648–658.

Bollner, C. (2006). Finger-tare (laminaria digitata). http://www.azote.se/image/Camilla-Bollner/Camilla-Bollner/5923/24. [Online; accessed October 13, 2016].

Comsol (2017). Turbulence modeling. https://www.comsol.com/blogs/which-turbulence-model-should-choose-cfd-application/. [Online; accessed May 31, 2017].

Cooper, G. G., Callaghan, F. M., Nikora, V. I., Lamouroux, N., Statzner, B., and Sagnes, P. (2007). Effects of flume characteristics on the assessment of drag on flexible macrophytes and a rigid cylinder. *New Zealand Journal of Marine and Freshwater Research*, 41(1):129–135.

Dingeldein, A. (2009). Cymathere triplicata. https://depts.washington.edu/fhl/mb/Cymathere_Andrea/Cymathere_home.html. [Online; accessed October 13, 2016].

Ennos, A. R. (1999). The aerodynamics and hydrodynamics of plants. *The Journal of experimental biology*, 202(Pt 23):3281.

Faltinsen, O. M. (1980). *Sea loads and motions of marine structures*. N.T.H-Trykk, Trondheim.

Flickr (2017). Strouhals vs. reynolds. `https://c1.staticflickr.com/3/2559/4150128499_4f176cd8d5_o.jpg`. [Online; accessed May 31, 2017].

Frostick, L. E., Thomas, R. E., Johnson, M. F., Rice, S. P., and McLelland, S. J. (2014). *Users Guide to Ecohydraulic Modelling and Experimentation : Experience of the Ecohydraulic Research Team (PISCES) of the HYDRALAB Network*. Users Guide to Ecohydraulic Modelling and Experimentation. Taylor and Francis, Hoboken.

Goring, D. G. and Nikora, V. I. (2002). Despiking acoustic doppler velocimeter data. *J. Hydraul. Eng.-ASCE*, 128(1):117–126.

Henry, P.-Y. (2016). *Parametrisation of aquatic vegetation in hydraulic and costal research : the importance of plant biomechanics in the hydrodynamics of vegetated flows*. Thesis.

Henry, P.-Y., Tørum, A., Øivind Artsen, Myrhaug, D., and Ong, M. C. (2012). Probability of exceeding the critical shear stress for sand motion in specific wave and current conditions. *Coastal Engineering Proceedings*, 1(33):4.

Hurd, C. L. (2000). Water motion, marine macroalgal physiology, and production. *Journal of Phycology*, 36(3):453–472.

Koehl, M. A. R. (1999). Ecological biomechanics of benthic organisms: Life history, mechanical design and temporal patterns of mechanical stress. *Journal of Experimental Biology*, 202(23):3469–3476.

Kregting, L., Blight, A., Elsäßer, B., and Savidge, G. (2013). The influence of water motion on the growth rate of the kelp laminaria hyperborea. *Journal of Experimental Marine Biology and Ecology*, 448:337–345.

Luhar, M. and Nepf, H. M. (2011). Flow-induced reconfiguration of buoyant and flexible aquatic vegetation. *Limnology and Oceanography*, 56(6):2003–2017.

Luhar, M. and Nepf, H. M. (2013). From the blade scale to the reach scale: A characterization of aquatic vegetative drag. *Advances in Water Resources*, 51:305–316.

Miler, O., Albayrak, I., Nikora, V., and O'Hare, M. (2012). Biomechanical properties of aquatic plants and their effects on plant–flow interactions in streams and rivers. *Research Across Boundaries*, 74(1):31–44.

Miler, O., Albayrak, I., Nikora, V., and O'Hare, M. (2014). Biomechanical properties and morphological characteristics of lake and river plants: implications for adaptations to flow conditions. *Research Across Boundaries*, 76(4):465–481.

Nepf, H. M. (2012a). Flow and transport in regions with aquatic vegetation. *Annual Review of Fluid Mechanics*, 44:123–42.

Nepf, H. M. (2012b). Hydrodynamics of vegetated channels. *Journal of Hydraulic Research*, 50(3):262–279.

Nikora, V., Wood, P. J., Rice, S. P., Little, S., Moir, H. J., and Vericat, D. (2010). Hydrodynamics of aquatic ecosystems : An interface between ecology, biomechanics and environmental fluid mechanics. *River Research and Applications*, 26(4):367–384.

Nortek AS (2016). Cymathere triplicata. `http://www.nortek-as.com/en`. [Online; accessed November 20, 2016].

Nortek AS (2017). Adv. `http://www.nortek-as.com/en`. [Online; accessed November 20, 2016].

Paul, M. and Henry, P.-Y. T. (2014). Evaluation of the use of surrogate laminaria digitata in eco-hydraulic laboratory experiments. *Journal of Hydrodynamics, Ser.B*, 26(3):374–383.

Pettersen, B. (2007). *Marin teknikk 3 : hydrodynamikk*. Marin hydrodynamikk. Marinteknisk senter, Institutt for marin teknikk, Trondheim.

Prof. John Southard (2006). Chapter 4: Flow in channels. `https://ocw.mit.edu/courses/earth-atmospheric-and-planetary-sciences/12-090-introduction-to-fluid-motions-sediment-transport-and-current-generated-sedim` [Online; accessed May 20, 2017].

Romsdals-Budstikke (2015). Tørket fingertare. `http://www.rbnett.no/incoming/article11886482.ece/6hovhv/BINARY/w980-adaptive/05FEADSC_0518.jpg`. [Online; accessed May 31, 2017].

Schiel, D. R. and Foster, M. S. (2015). *The Biology and Ecology of Giant Kelp Forests*. Giant kelp forests. University of California Press, Berkeley.

Schlichting, H. and Gersten, K. (2017). *Boundary-Layer Theory*. Springer Berlin Heidelberg: Berlin, Heidelberg, Berlin, Heidelberg.

Seckbach, J., Einav, R., and Israel, A. (2010). *Seaweeds and their Role in Globally Changing Environments*, volume v.v. 15 of *Cellular Origin, Life in Extreme Habitats and Astrobiology, 15*. Springer, Dordrecht.

Sjøtun, K., Olsen, B. R., and Eggereide, S. F. (2004). *Biomassekartlegging av Laminaria digitata i Smøla-området = Biomass survey of Laminaria digitata in the Smøla area*, volume nr 11-2004 of *Biomass survey of Laminaria digitata in the Smøla area*. Havforskningsinstituttet, Bergen.

Steen, S., Norges teknisk-naturvitenskapelige universitet Marinteknisk, s., and Norges teknisk-naturvitenskapelige universitet Institutt for marin, t. (2014). *Experimental methods in marine hydrodynamics : compendium*. Experimental methods in marine hydrodynamics : TMR7 : lecture notes. Akademika forlag Kompendieforlaget, Trondheim, rev. ed. edition.

Thomas, R. E., Johnson, M. F., Frostick, L. E., Parsons, D. R., Bouma, T. J., Dijkstra, J. T., Eiff, O., Gobert, S., Henry, P.-Y., Kemp, P., McLelland, S. J., Moulin, F. Y., Myrhaug, D., Neyts, A., Paul, M., Penning, W. E., Puijalon, S., Rice, S. P., Stanica, A., Tagliapietra, D., Tal, M., Tørum, A., and Vousdoukas, M. I. (2014). Physical modelling of water, fauna and flora: knowledge gaps, avenues for future research and infrastructural needs. *Journal of Hydraulic Research*, 52(3):311–325.

Tiwari, B. K. and Troy, D. (2015). *Seaweed Sustainability : Food and Non-Food Applications*. Elsevier Science, Burlington.

Voulgaris, G., Trowbridge, J., and Voulgaris, G. (1998). Evaluation of the acoustic doppler velocimeter (adv) for turbulence measurements. *Journal of Atmospheric and Oceanic Technology*, 15(1, pt. 2):272–289.

Wahl, T. L. (2004). *Analyzing ADV Data Using WinADV*, pages 1–10.

Whittaker, P., Wilson, C. A. M. E., and Aberle, J. (2015). An improved cauchy number approach for predicting the drag and reconfiguration of flexible vegetation. *Advances in Water Resources*, 83:28–35.

Çengel, Y. A., Cimbala, J. M., and Kanoğlu, M. (2010). *Fluid mechanics : fundamentals and applications*. McGraw-Hill, Boston, 2nd ed. in si units. edition.

Appendix A

Surrogate model motions

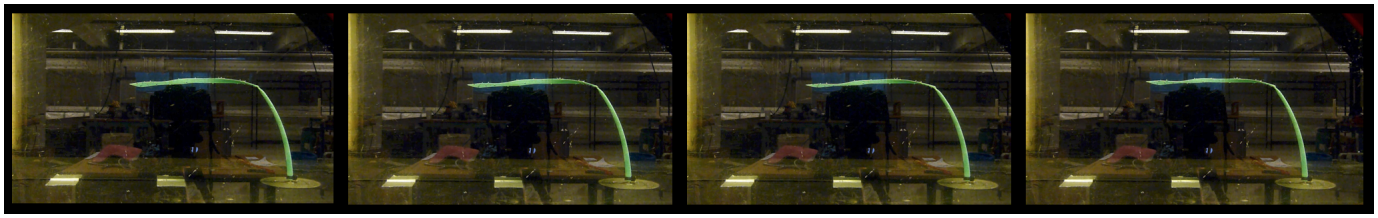

(a)

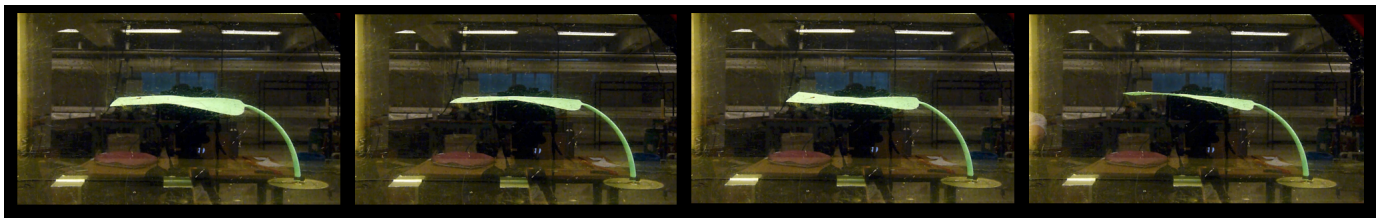

(b)

(c)

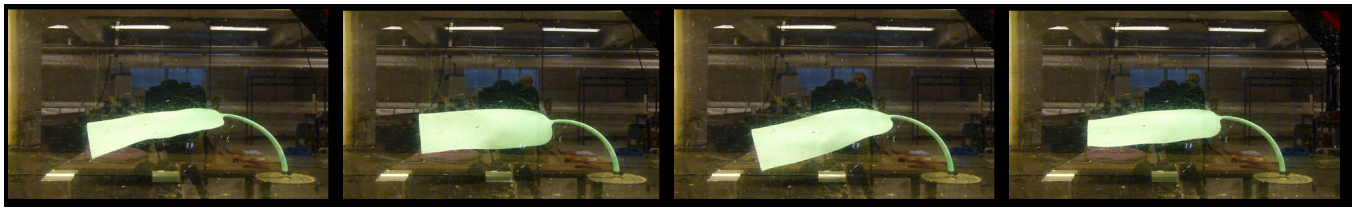

(d)

Figure A.1: Motions from the model test of the surrogate 20A (a) *0.05 m/s*, (b) *0.14 m/s*, (c) *0.17 m/s*, and (d) *0.21 m/s*.

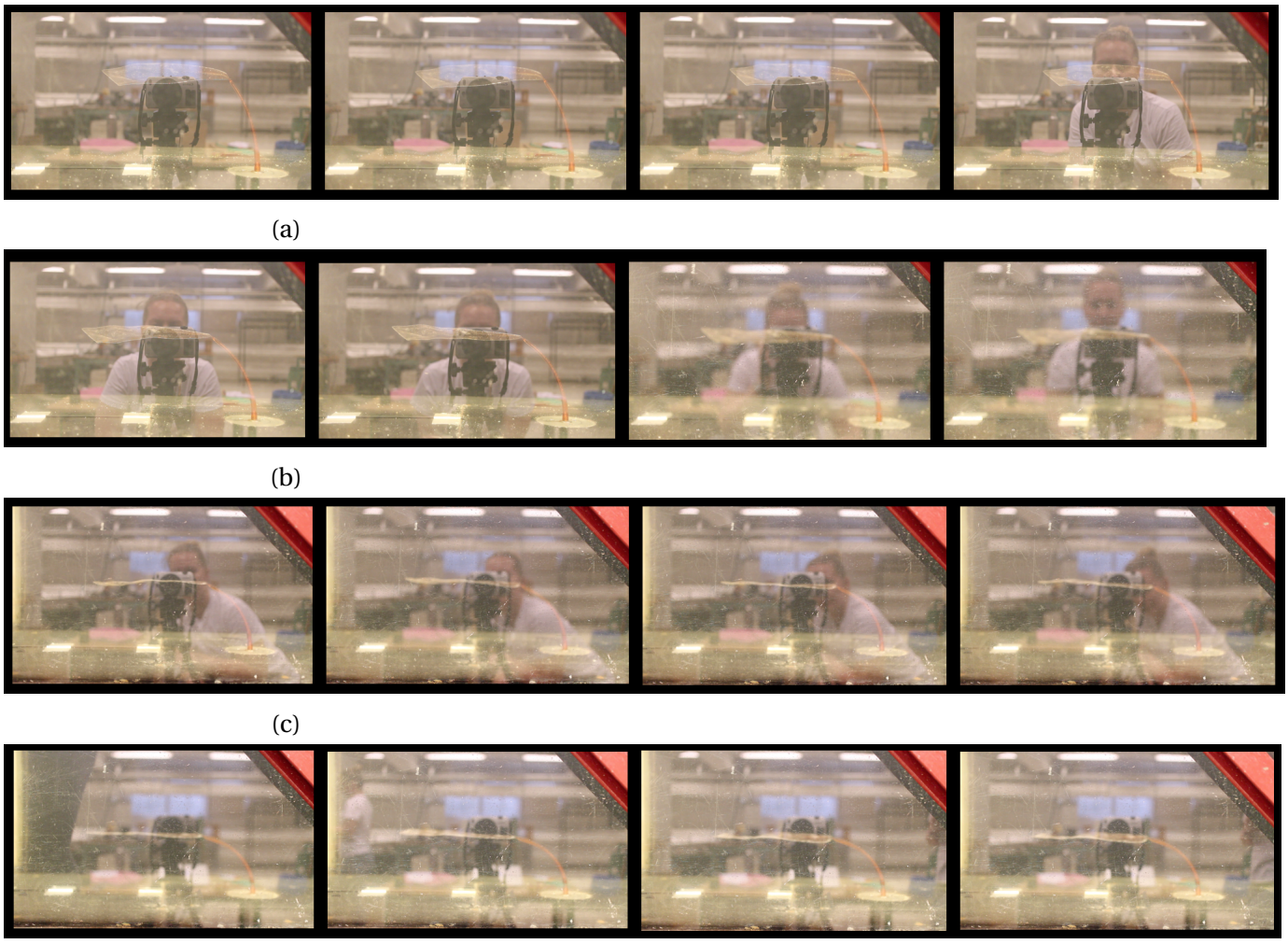

(a)

(b)

(c)

(d)

Figure A.2: Motions from the model test of the surrogate 60A (a) *0.05 m/s*, (b) *0.14 m/s*, (c) *0.17 m/s*, and (d) *0.21 m/s*.

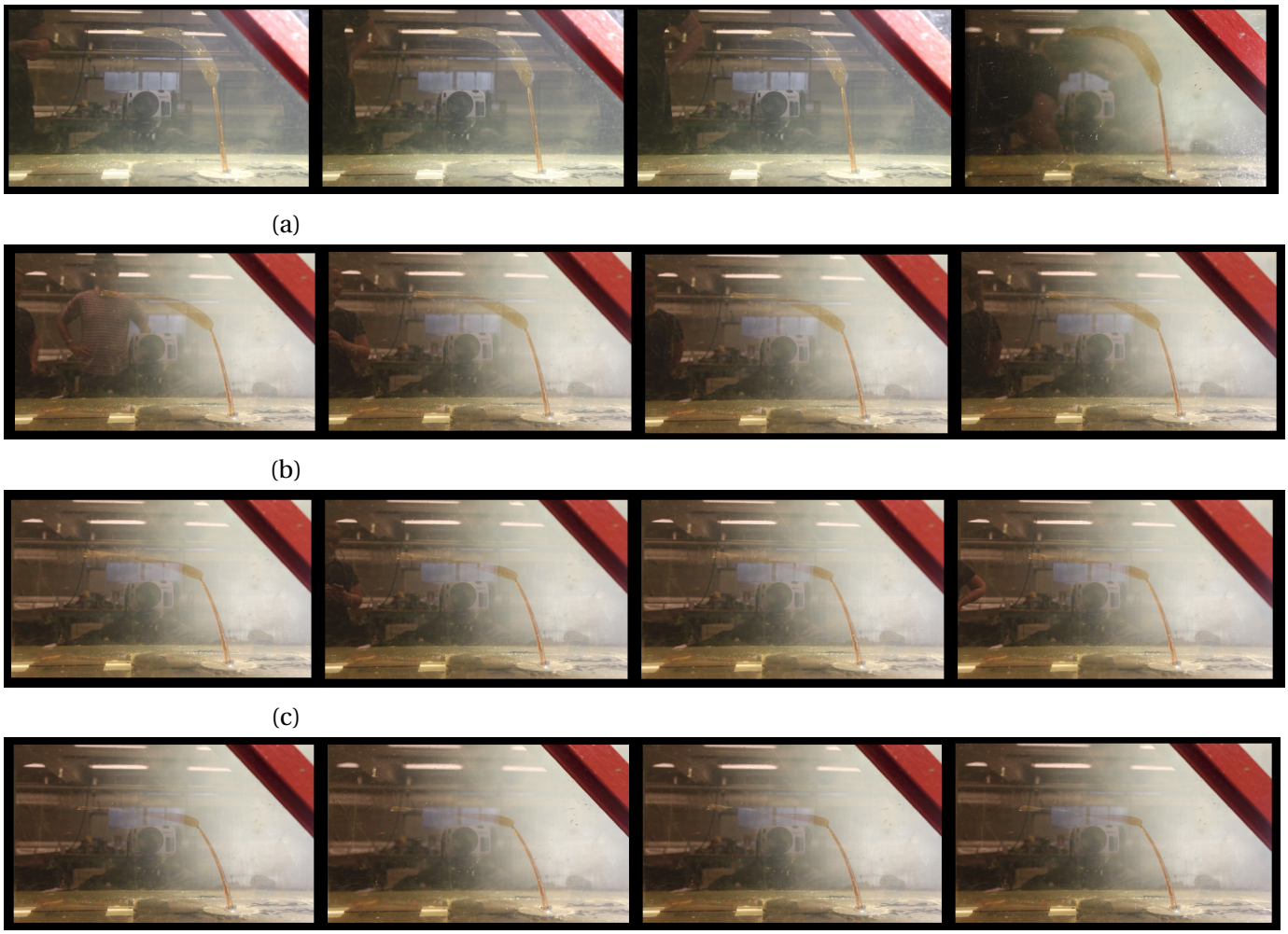

(a)

(b)

(c)

(d)

Figure A.3: Motions from the model test of the surrogate 90A (a) *0.05 m/s*, (b) *0.14 m/s*, (c) *0.17 m/s*, and (d) *0.21 m/s*.

Appendix B

Technical specification ADV

Technical Specifications

Water Velocity Measurements	
Range:	±0.01, 0.1, 0.3, 1, 2, 4 m/s*)(user selectable)
Accuracy:	±1% of measured value ±1 mm/s
Sampling rate (output):	1–25 Hz (standard firmware), 1–200 Hz (Plus firmware)

*) The velocity range is not the same in the horizontal and vertical direction. Please refer to the configuration software.

Sampling Volume	
Distance from probe:	0.05 m
Diameter:	6 mm
Height (user selectable):	3–15 mm
Echo Intensity	
Acoustic frequency:	10 MHz
Resolution:	Linear scale
Dynamic range:	25 dB
Sensors	
Temperature:	Thermistor embedded in probe
Range:	–4°C to 32°C
Accuracy/Resolution:	1°C/0.1°C 5
Time response:	min
Data Communication	
I/O:	RS 232. The software supports most commercially available USB–RS 232 converters.
Communication Baud rate:	300–115 200 Baud
User control:	Handled via Vectrino Win32® software, ActiveX® function calls, or direct commands.
Analog outputs:	3 channels standard, one for each velocity component.
Output range:	0–5 V, scaling is user selectable.
Synchronization:	SynchIn and SynchOut
Multi Unit Operation	
Software:	Polysync
I/O:	RS 232–USB support for devices with 1, 2, 4, and 8 serial ports.
Software ("Vectrino")	
Operating system:	Windows®XP, Windows®7
Functions:	Instrument configuration, data collection, data storage. Probe test modes.

Power	
DC Input:	12–48 VDC
Peak current:	2.5 A at 12 VDC (user selectable)
Max. consumption:	200 Hz 1.5 W
Connectors	
Bulkhead:	MCBH-12-FS, bronze (Impulse)
Cable:	PMCIL-12-MP – see also options below.
Materials	
Standard model:	Delrin® housing. Stainles steel (316) probe and screws.
Environmental	
Operating temperature:	–4°C to 40°C
Storage temperature:	–15°C to 60°C
Shock and vibration:	IEC 721-3-2
Dimensions	
See drawings on page 2-3 for dimensions	
Weight in air:	1.2 kg
Weight in water:	Neutral

Options

- Standard or Vectrino Plus firmware
- 4-beam down-looking probe or side-looking probe. Fixed stem or flexible cable
- 10, 20, 30 or 50 m cable with Impulse underwater connector
- RS 232–USB converter (one-to-one, four-to-one or eight-to-one)
- Combined transportation and storage case

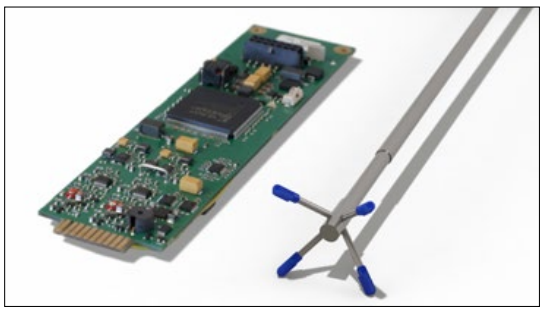

The Vectrino consists of two basic elements: the probe attached to a clyndrical housing and the processor inside the housing. From here the processed data is sent over a serial line or analog signals can be sent to an A/D converter.

TS-060-en-01-2017

Appendix C

Technical specification F/T Sensor

Single-Axis Overload	
Fxy	±250 N
Fz	±480 N
Txy	±1.6 Nm
Tz	±1.8 Nm
Stiffness (Calculated)	
X-axis & Y-axis forces (Kx, Ky)	8.2×10^6 N/m
Z-axis force (Kz)	1.1×10^7 N/m
X-axis & Y-axis torque (Ktx, Kty)	2.4×10^2 Nm/rad
Z-axis torque (Ktz)	3.8×10^2 Nm/rad
Resonant Frequency	
Fx, Fy, Tz	2200 Hz
Fz, Tx, Ty	2200 Hz
Physical Specifications	
Weight*	0.0408 kg
Diameter*	20.1 mm
Height*	22.2 mm

** Specifications include standard interface plates.*

Figure C.1: Technical specifications of the F/T sensor used in the experimental testing.